JOURNAL OF GEOPHYSICAL RESEARCH, VOL. 108, NO. A10, 1356, doi:10.1029/2002JA009657, 2003

Correction published 7 July 2004

Estimated errors in magnetic cloud model fit parameters with force-free cylindrically symmetric assumptions

R. P. Lepping,[1] D. B. Berdichevsky,[2] and T. J. Ferguson[1,3]

Received 22 August 2002; revised 13 March 2003; accepted 9 June 2003; published 8 October 2003.

[1] This paper briefly reviews our earlier study done on estimated errors in various output fit parameters resulting from a specific force-free interplanetary magnetic cloud model [*Lepping et al.*, 1990], applied to randomly noised-up fields of simulated clouds, and shows that such random noise simulation studies are inadequate. It then proceeds to carry out an error study of the same model output parameters on the basis of more realistic input magnetic field noise sets derived from actual clouds observed in WIND data over the years 1995 to 1998. In this part of the study, 1824 "noised-up" simulated clouds are produced for use in the same force-free cloud model to study the spread in values for each of 7 model parameters, plus associated quantities, as a function of noise level. Four noise levels are used with RMSs of 0.5, 2.0 (typical level), 3.0, and 4.0 nT per field component of input bias-free fluctuation fields. These are based on manipulation of difference fields from 19 actual magnetic clouds, where a difference field is defined as the vector difference between the observational field and that from the original model fit for each actual cloud. The averages and RMSs of 240 output (model fit) parameter distributions are produced and discussed. The study determines how the model fit parameters, and especially their distributions, vary as a function of various input noise levels and of the resulting least squares $(\chi^2)^{\frac{1}{2}}$ values for various exact input parameters, such as the cloud's axial attitude and the closest approach distance of the spacecraft. Practical goals were to better understand the fit program's limitations and to provide a prescription for estimating future errors in specific magnetic cloud (and probably magnetotail flux rope) fittings. The degree of symmetry in the model solution is used along with $(\chi^2)^{\frac{1}{2}}$ to judge the quality of the fit. *INDEX TERMS:* 2109 Interplanetary Physics: Discontinuities; 2134 Interplanetary Physics: Interplanetary magnetic fields; 2164 Interplanetary Physics: Solar wind plasma; *KEYWORDS:* magnetic clouds, magnetic fields, solar wind, force free, WIND

Citation: Lepping, R. P., D. B. Berdichevsky, and T. J. Ferguson, Estimated errors in magnetic cloud model fit parameters with force-free cylindrically symmetric assumptions, *J. Geophys. Res.*, *108*(A10), 1356, doi:10.1029/2002JA009657, 2003.

1. Introduction

[2] A magnetic cloud is defined in terms of in situ spacecraft measurements of magnetic fields and particles in the interplanetary medium. It is a structure in the solar wind having: (1) enhanced magnetic field strength, (2) a smooth change in field direction as observed by a spacecraft passing through the cloud and (3) low proton temperature compared to the ambient proton temperature [*Burlaga*, 1988, 1995]. Magnetic clouds are understood to be usually large structures, so that their durations are long, between about 10 and 48 hours at 1 AU, averaging about 1 day in duration. The global nature of a magnetic cloud has been verified through observations and analysis of data from multiple spacecraft [*Burlaga et al.*, 1990]. These large transient structures are believed to originate from erupting prominences on the Sun [*Bothmer and Schwenn*, 1994; *Schwenn*, 1996], and some of their specific properties have been successfully correlated with detailed solar features [*Marubashi*, 1997]. They are important in studying solar terrestrial effects generally, especially because of the high probability of their causing geomagnetic storms and other effects at Earth [*Kamide et al.*, 1997; *Tsurutani and Gonzalez*, 1997]. Over the years many models have been used to fit the magnetic field structure of interplanetary magnetic clouds when the clouds appeared to satisfy a magnetic flux rope geometry [see, e.g., *Burlaga*, 1995; *Marubashi*, 1986; *Lepping et al.*, 1990; *Farrugia et al.*, 1992, 1999; *Osherovich et al.*, 1993, 1995; *Shimazu and Vandas*, 2002; *Berdichevsky et al.*, 2003]. For proper quantitative comparisons of the solar interplanetary connection and the interplanetary magnetosphere connections, when magnetic clouds are observed, knowing the accuracy of resulting cloud model output parameters is usually important. However, no quantitative analyses of any of these models in terms of typical estimates of the errors on their fit parameters have been done to this date in a systematic way. We try to rectify this

[1]Laboratory for Extraterrestrial Physics, NASA Goddard Space Flight Center, Greenbelt, Maryland, USA.
[2]L-3 Communications, EER Systems, Inc., Largo, Maryland, USA.
[3]Also at Linganore High School, Frederick, Maryland, USA.

0148-0227/03/2002JA009657

here, at least with respect to one common magnetic cloud model, by studying the resulting errors on the model's fit parameters as a function of the level of the amplitude of field fluctuations ("noise level") within a cloud superimposed on the field of an otherwise exactly simulated flux rope according to that same model. This fluctuating field may be considered a perturbation field. A corresponding output measure of the quality of the cloud fit to data, specifically χ^2 (but there are others, discussed below), is also compared to the input noise level. The study is primarily an analysis of the accuracy of the specific model that we have been using for many years, the static force-free (constant α) cylindrically symmetric model [*Burlaga*, 1988; *Lepping et al.*, 1990], but it also provides a practical prescription for estimating the kind of error addressed here for any magnetic cloud analyzed in the future, provided the model employed here is a good approximation to the actual cloud's field structure. In that respect, the results of the study should be useful for estimating errors in flux rope modeling parameters generally (i.e., for noncloud flux ropes, such as those observed in the magnetotail [e.g., *Lepping et al.*, 1996] or small-scale (1-hour) interplanetary flux ropes [e.g., *Moldwin et al.*, 2000], with judicious application.

[3] There are many possible sources of error in modeling magnetic clouds. We list the most obvious ones here: (1) noise fluctuations in the IMF within the cloud (meaning perturbing fields), (2) incorrect choice of cloud boundaries, (3) not accounting for systematic features in violation of the model (e.g., those due to cloud expansion [*Osherovich et al.*, 1993], noncircular cross section [*Lepping et al.*, 1998], interaction of the cloud with surrounding plasma, etc.), (4) measurement errors in **B** and the velocity (**V**) of the cloud, and finally, not to forget the obvious, (5) misidentification of the structure as a flux rope in the first place which includes the possibility of a misidentification of multiple flux ropes as a single magnetic cloud. (Strictly speaking (5) could have been considered part of (2).) There are generally objective means of obtaining the likelihood that we are identifying a magnetic cloud; e.g., examination of the full plasma and field data sets together, along with solar energetic particles, usually gives confidence that a candidate is, or is not, a flux rope, but 5 could, for any given case, clearly be an important source of error. And 4 can almost always be ignored compared to sources 1 and 2, which for most magnetic clouds are the greater sources of error. Source 2 is usually important, but we concentrate here on 1 as being important and the most tractable. If there is doubt in the choice of the boundary positions, the modeler can always try many reasonable attempts at start and end times, and note the average and variation in output parameters which should reflect the degree of uncertainty due to this source of error. This error source may be considerable for what may be called "unstable" cases (where small changes in boundary candidates give large changes in output parameter values), for which poor results are expected. We should point out that the detailed features in the plasma parameters, especially proton temperature and proton beta, and even bulk speed (although not part of a cloud's definition), are useful in choosing the proper boundaries. And the presence of field directional discontinuities is usually definitive in choosing boundaries in that a significant directional discontinuity (DD) should not exist within the cloud, and therefore the closest DD may be the boundary. And sometimes a dip in $|\mathbf{B}|$, appearing as a magnetic hole, will be seen at one or both boundaries giving considerable help in making a proper choice [*Farrugia et al.*, 2000]. Detail treatment of error source 3 is beyond the scope of this study, but it is not completely independent of source 1, because "noise fluctuations" is a relative term, which, in fact, depends on the choice of model. As the model becomes more complex and attempts to account for more systematic features, such as cloud expansion, part of a simpler model's noise fluctuation becomes part of the more complex model's field. In a sense, the more sophisticated model should then, at least in principle, have lower amplitude noise to accommodate for any given cloud compared to the simpler model. For a simple model, such as the static force free of constant α, which we are concerned with here, all systematic deviations from the model field (i.e., sources 1 and 3) are lumped together into the term fluctuation noise; later we call this "trend" noise.

[4] Hence each of the many simulated flux ropes to be generated and subsequently used in this study will consist of the superposition of two vector fields: an exactly simulated (ES) flux rope field ($\mathbf{B_{ES}}$), generated from the constant alpha force-free cylindrically symmetric model (the ideal rope) plus an unbiased fluctuating field ($\mathbf{B_N}$), emulating noise (N). In the main part of this study the fluctuating field is derived from difference fields, i.e., between field observations from actual magnetic clouds of flux rope structure and model fields derived from least squares fits to these clouds using the model of *Lepping et al.* [1990], as pointed out. (We also briefly address the random noise field and its consequences.) Since these difference fields are residual fields from the fitting process, they are "noise" with respect to the model. The field observations are from the MFI magnetometer [*Lepping et al.*, 1995] on the WIND spacecraft for magnetic clouds identified over the years 1995 to 1998. The seven magnetic cloud model fit parameters to be examined are: the cloud's axial field strength (B_O), the direction of the cloud's axis in terms of a longitude (ϕ_A) and latitude (θ_A), the cloud's diameter ($2R_O$), relative closest approach distance of the spacecraft (C.A.D. $\equiv Y_O$), closest approach time (t_o), and rope handedness (H). The specific procedure is described below.

[5] In the *Lepping et al.* [1990] technique a least squares fit of functions that properly describe the force-free field ((2) below) is initially made to unit-normalized observed magnetic field averages. Hence at first only the field's direction is considered to find the cloud's geometrical properties, i.e., all but B_O and handedness. (A simple linear scaling of the model field's magnitude to the observed field's magnitude is done later to obtain the proper magnitude of the axial field, B_O.) A "reduced" chi-square to the fit, χ^2_R = chi-square/(3n − N), where n is the number of hour average points and N = 5 is the number of parameters in this part of the fit, is used, among other parameters that consider cloud symmetry, to measure the "quality" of the fit. Below we refer to χ^2_R as simply χ^2 everywhere for simplicity since 3n − 5 in this study will be a fixed value. Because the magnetic fields were unit-normalized χ^2 is dimensionless. Appendix A describes how the least squares fitting to the normalized field is carried out.

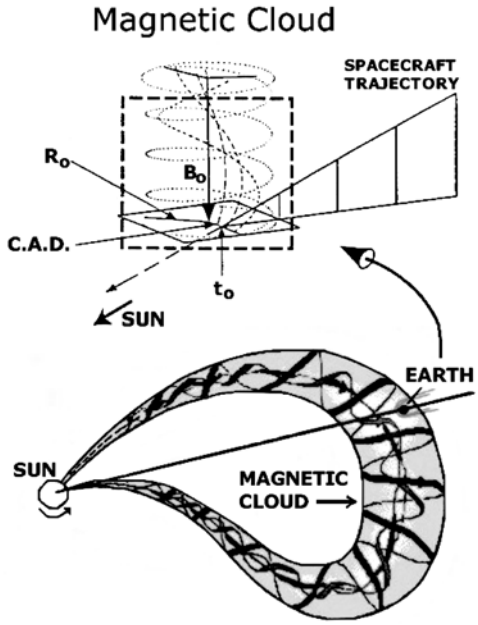

Figure 1. (top) A sketch of the local magnetic field structure of the idealized cloud as observed by a near-Earth spacecraft in relative motion with respect to the cloud. The field structure is assumed to be a nested set of field lines on various cylinders from the innermost of zero radius, where the field is parallel to the axis, to that on the boundary of radius R_O, where the field is perpendicular to the axis. The sketch defines some (4) of the quantities used in the cloud fitting program of *Lepping et al.* [1990]: B_O is the value of the magnetic field on the cloud's axis, R_O is the cloud's radius, C.A.D is the spacecraft's closest approach distance (also called Y_O) to the axis, and t_o is closest approach time. The other (3) fit parameters are θ_A, ϕ_A (giving axial attitude), and handedness (H); see the text. The magnetic cloud in general is not assumed to be symmetric about the Sun-Earth line in the model. (bottom) An idealized magnetic cloud (based on the work of *Marubashi* [1997]) on a global scale reaching 1 AU; see a similar model by *Burlaga et al.* [1990].

[6] The value of χ^2 for each event will be examined as a function of noise level, along with two intermediate model parameters ($\Delta\theta_A$, $\Delta\phi_A$, as in Appendix A) that measure how well the fit functions are converging. This gives 10 parameters that will be examined. By having many noise sets available to add to a given ideal flux rope, of exactly known characteristics, we have the ability to generate many noised-up clouds to which the *Lepping et al.* [1990] model can be applied. Hence output parameter value distributions can be created, their averages determined, and their root mean square deviations (RMSs) obtained. Parameter uncertainties are then estimated according to the spread (RMS) in any given parameter distribution. This is done in the spirit of the Monte Carlo technique [e.g., *Rubinstein*, 1981; *Metropolis*, 1985; *Sobol'*, 1994]. That is, it is a statistical study of the variations in output fit parameters (in terms of output σs) from the propagation through a magnetic cloud model of variations in (input) noise, $\mathbf{B_N}$, for various conditions and a large number of cases. The output σs are then interpreted as levels of uncertainties or errors on the average fit parameter values.

[7] An earlier attempt to randomly "noise up" exactly simulated magnetic clouds for the purpose of carrying out a similar error study was made by *Lepping et al.* [1998], but that work gave results of limited applicability. Nevertheless, those results will be briefly discussed, before the more realistic results of this study are developed.

2. Magnetic Cloud Simulations With Random Noise

[8] *Lepping et al.* [1998] described a study to estimate magnetic cloud parameter errors based on the fields ($\mathbf{B_S}$) of simulated magnetic clouds developed on the basis of exactly simulated fields ($\mathbf{B_{ES}}$) plus random noise fields ($\mathbf{B_{RN}}$) for various noise levels. That is,

$$\mathbf{B_S} = \mathbf{B_{ES}} + \mathbf{B_{RN}}, \tag{1}$$

where $\mathbf{B_{ES}}$ is the *Lundquist* [1950] Bessel function solution [$J_O(\alpha r)$, $J_1(\alpha r)$] to the constant α, cylindrically symmetric, force-free flux rope, i.e., the solution to $\nabla^2\mathbf{B} = -\alpha^2\mathbf{B}$ in cylindrical coordinates [see *Priest*, 1990; *Goldstein*, 1983]:

$$B_{ES,A} = B_O J_O(\alpha r), \quad B_{ES,T} = H\, B_O J_1(\alpha r), \quad \text{and} \quad B_{ES,R} = 0, \tag{2}$$

which are functions of only the radial distance from the rope's axis, r, where the subscripts A, T, and R refer to axial, tangential and radial components, respectively. Figure 1, which shows a picture of an idealized magnetic cloud (flux rope), through which a spacecraft is passing, describes four of the fundamental quantities by which the rope is described. (The relative motion of cloud and spacecraft, in a GSE coordinate system, for example, is almost fully due to the cloud's motion since the observing spacecraft moves slowly compared to the cloud in that system. Hence the spacecraft's motion is neglected.) There are a total of seven fit parameters. The other three quantities are the rope's axial attitude, given in terms of its axial latitude, θ_A, and longitude, ϕ_A, and the handedness, H, of the helical field, where H is + 1 or − 1, for right-handed or left-handed, respectively. Notice that when $\alpha r = 2.4$, $J_O(2.4)$ is 0.0 (i.e., $B_{ES,A}$ is 0.0), a desirable place to choose the boundary as previously argued [*Burlaga*, 1995; *Lepping et al.*, 1990]; at that radial position the cloud's field is purely tangential, i.e., it is where $B_{ES,T}$ reaches a local maximum. Hence in magnetic cloud parameter fitting $2.4/\alpha$ ($\equiv R_O$) is chosen as the radius of the magnetic cloud, with rare exceptions, such as a few cases where the cloud has an apparent core and annulus structure. Figure 2 shows an example (the 9 June 1997 case) of the use of such a model to fit a WIND magnetic cloud, in terms of a profile of cloud observations (dots are 1-hour averages) in Cartesian components ($B_{X,Y,Z}$) and magnitude (B) and angular representation (field latitude, θ_B, and longitude, ϕ_B); the solid curves are the model representation from (2) rendered in GSE coordinates. In this case the fit parameters were: duration = 22 hours, $\sqrt{\chi}^2 = 0.0196$, (asymmetry factor 6.4%, defined below (11), which depends on t_o), $B_O = 15.0$ nT, $\theta_A = 219°$, $\theta_A = -17°$, $Y_O/R_O = 0.53$, $2R_O = 0.193$ AU, and H = left-handed. Concerning quality of

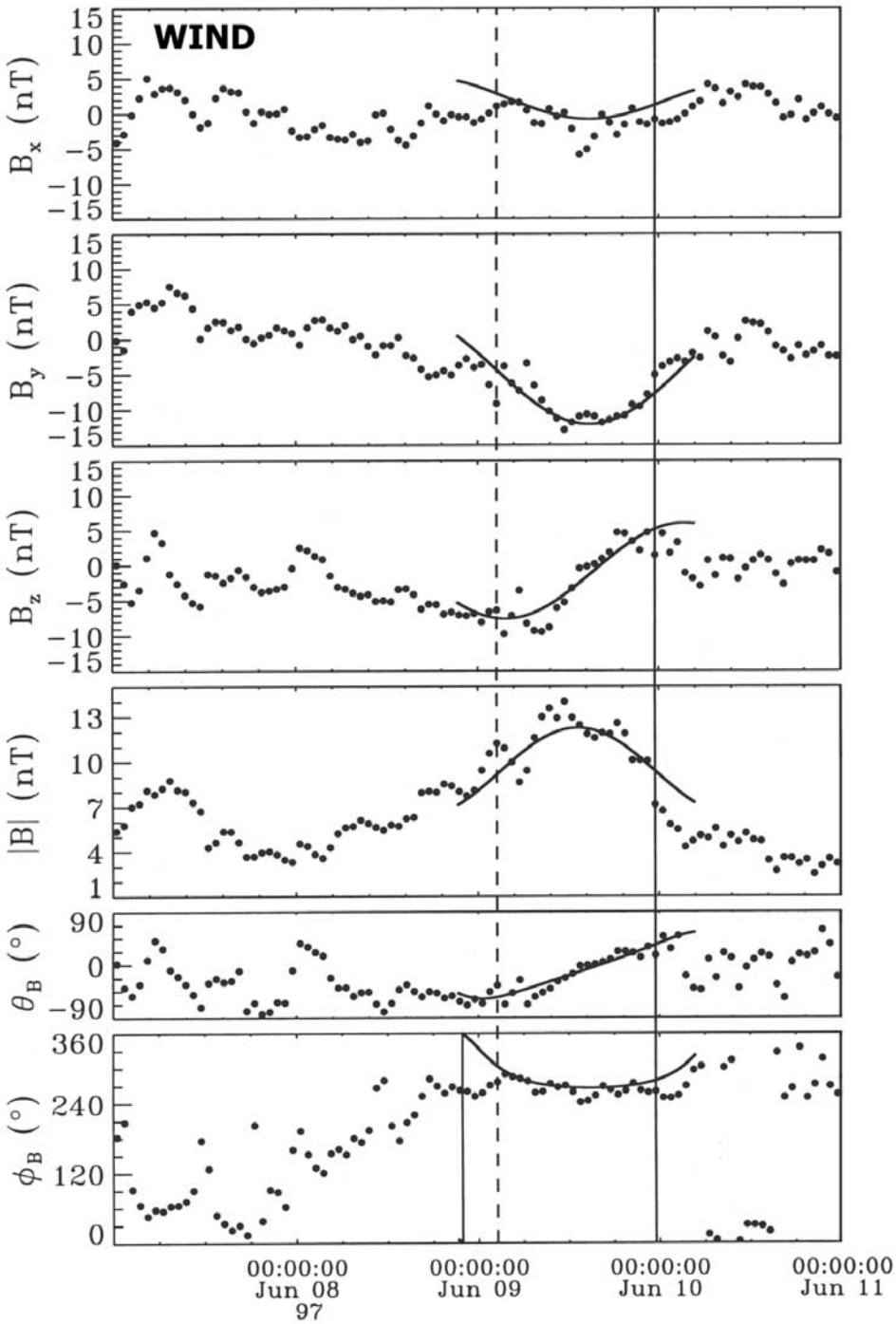

Figure 2. WIND 1-hour magnetic field observations (dots), in GSE coordinates, around time of a magnetic cloud of 9 June 1997, in terms of components (B_X, B_Y, B_Z; top 3 panels), B (field magnitude), θ_B (field latitude), and ϕ_B (field longitude); day 160 is 9 June. The solid curve is the cloud model fit of the data between the vertical lines representing the start (dashed) and end (solid) times of the cloud. The solid curves are shown outside the vertical lines only for comparison to noncloud observations. The fit was very symmetrical with an excellent A.S.F of 6% (see (11) below).

fit, $\sqrt{\chi^2}$ was 0.0196, which is moderately higher than typical values. All panels of Figure 2 show the field observations markedly fluctuating around the model curves, with "wavelengths" sometimes of many hours, being especially clear for B_Y, B_Z and θ_B. The cloud is close to average with regard to size ($2R_O$), field strength (B_O) at 1 AU, and the quality of fit (according to $\sqrt{\chi^2}$ and ASF), and the magnitude fit is slightly better than typical cases.

[9] Table 1 displays one aspect of the results of the simulations in terms of χ^2 (in the form of $\sqrt{\chi^2}$) quantized

Table 1. Random Noise Levels Versus Output $\sqrt{\chi^2}$

For Y_O/R_O = 0%			For Y_O/R_O = 45%			For Y_O/R_O = 90%		
h[a]	v_{IR}, nT	$\sqrt{\chi^2}$	h[a]	v_{IR}, nT	$\sqrt{\chi^2}$	h[a]	v_{IR}, nT	$\sqrt{\chi^2}$
0.0	0.0	0.0000	0.0	0.0	0.0000	0.0	0.0	0.0004
0.5	1.0	0.0046	0.5	1.0	0.0052	0.5	1.0	0.0097
1.0	2.0	0.0093	1.0	2.0	0.0104	1.0	2.0	0.0118
2.0	4.0	0.0185	2.0	4.0	0.0211	2.0	4.0	0.0361[b]
4.0	8.0	0.0372[b]	4.0	8.0	0.0416[c]	4.0	8.0	0.0472[c]

[a]Where h is a noise level, and v_{IR} (nT) = h B_O σ_O (where B_O = 16.4 nT and σ_O = 0.123).
[b]Marginally acceptable value.
[c]Not an acceptable value.

for various values of input noise levels (h) and values of Y_O/R_O, where

$$v_{IR}(\text{nT}) = \text{h } B_O \ \sigma_O, \tag{3}$$

and where B_O = 16.4 nT, an average axial value [see *Lepping and Berdichevsky*, 2000], and σ_O = 0.123, a typical input noise sigma (which is discussed below); expressed this way σ_O can be given as a dimensionless quantity, a consistent approach since it was derived from cloud difference fields that were B_O-normalized. Hence h = 1 is a typical noise level giving v_{IR} = 2 nT from (3). Three different

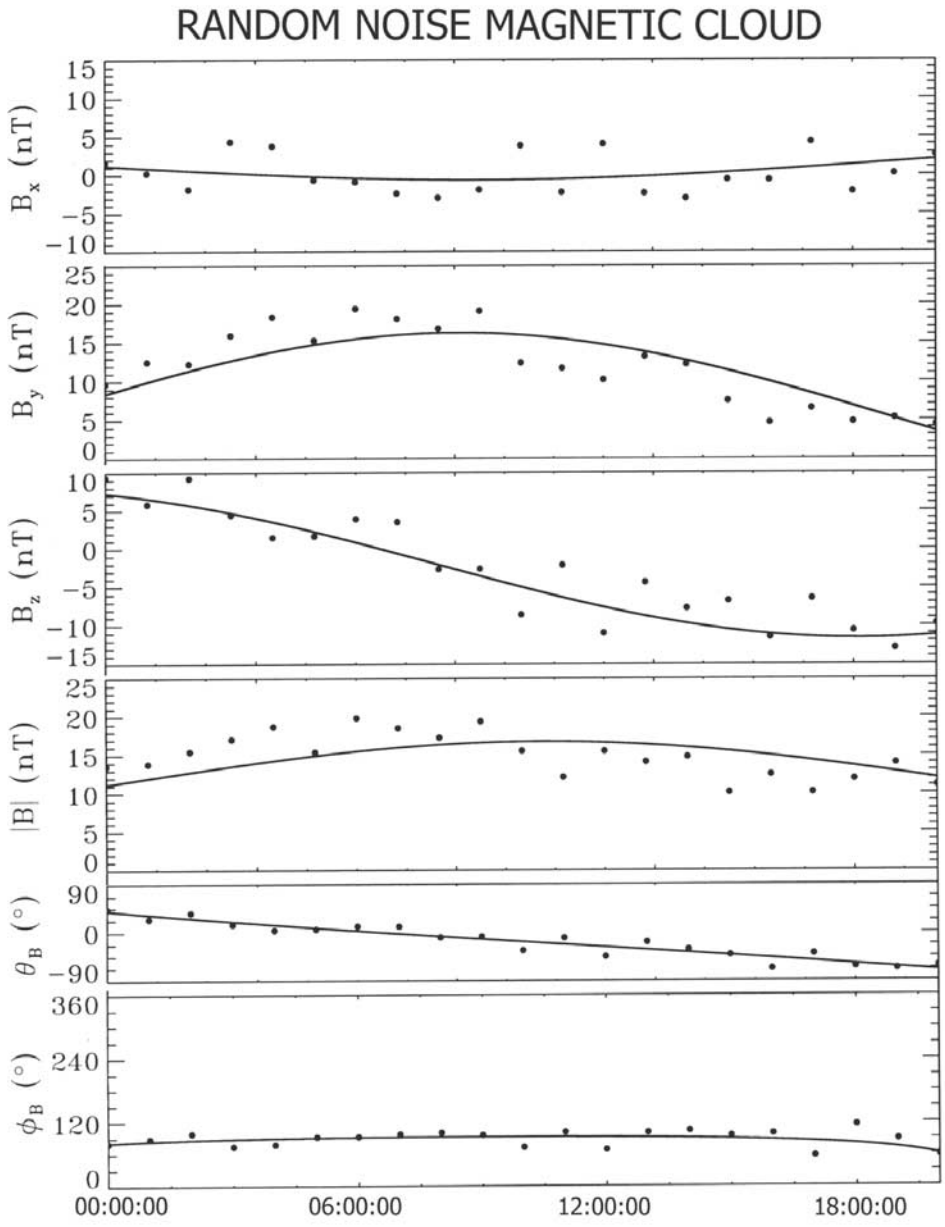

Figure 3. An example of a simulated magnetic cloud, in the same format as that of Figure 1, developed from random noise and showing an unrealistic profile. The observations (dots) are assumed to occur once every hour. The measure of cloud parameter fitting, $\sqrt{\chi^2}$ (see text), is 0.0197, which is only slightly higher than typical values encountered. The noise appears as a band of random variations around the fitted curve, unlike realistic cases.

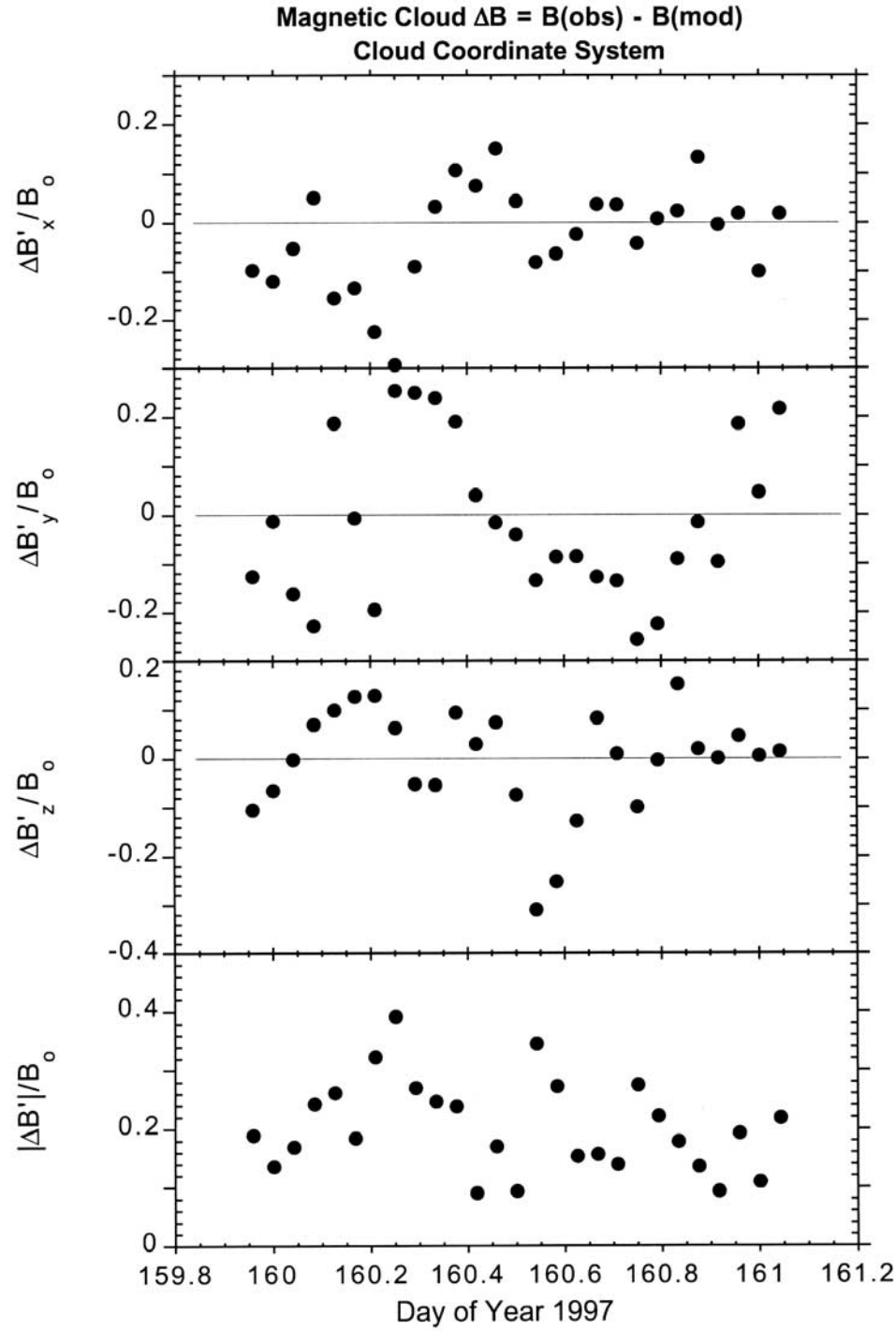

Figure 4. The time profile of the difference field (i.e., $\mathbf{\Delta B} = \mathbf{B_{OBS}} - \mathbf{B_M}$, where $\mathbf{B_{OBS}}$ is the WIND observed field and $\mathbf{B_M}$ is the model-estimated field) normalized by $B_{O,}$ for the 9 June 1997 magnetic cloud, all rendered in cloud coordinates (shown by primes); see text for definition of the magnetic cloud coordinates. B_O is the model-estimated field on the cloud's axis.

closest approach distances were considered (Y_O/R_Os of 0, 45 and 90%, representing ever shorter paths across a cloud as Y_O/R_O increases). As expected, Table 1 shows that, for a fixed Y_O/R_O, as h increases $\sqrt{\chi^2}$ increases, and, in fact, it does so linearly. Also for a fixed h, $\sqrt{\chi^2}$ increases as Y_O/R_O increases, finally to an unacceptably large value of $\sqrt{\chi^2} = 0.05$. To obtain realistic levels of variation in the output fit parameters it was sometimes necessary to use amplitudes of input noise (v_{IR}) that represented two times sigma, yielding only moderately high values of $\sqrt{\chi^2}$ (i.e., about 0.018 to 0.020), i.e., corresponding to h = 2 (or v_{IR} = 4 nT). This gave what in essence was a uniform noise band around the ideally simulated cloud field at a "frequency" that was much too high to represent real noise, which

appears to have lower frequency components or trend-like noise. Figure 3 shows an example of what a typical to moderately high noised-up simulated cloud looks like when such random noise is used. It does not appear to give a realistic profile. For example, it shows field variations within bands around the fitted values (solid curve), especially clear in B_Z and θ_B, rather than the usual smooth lower frequency wave-like noise variations encountered in real clouds (as in Figure 2). The random noise case also required a relatively high noise level h of 2.0 (v_{IR} = 4 nT), but its output $\sqrt{\chi^2}$ (0.0197) was only moderately higher than typical values encountered for actual cases. We list here the related program-estimated values for the fit parameters (versus {exact input values}) for Figure 3's simulation: B_O = 17.9 nT {17 nT}, R_O = 0.12 AU {0.13 AU}, $\theta_A = -19°$ {0.0°}, $\phi_A = 115°$ {90°}, $Y_O/R_O = -0.30$ {0.0}, H = right-handed, ASF = 4.7%(excellent).

[10] The value of this part of the study was that it showed that simulated magnetic clouds with legitimate uncertainty estimates of output fit parameters cannot be realistically accomplished with random noise. However, it did yield some useful qualitative information concerning the relationship between the sigmas of the input field (reflected by v_{IR}) and the output-$\sqrt{\chi^2}$, parameterized by Y_O/R_O, from application of the *Lepping et al.* [1990] program.

3. "Trend Noise" Simulations

[11] From the unsatisfactory results of the random noise study we searched for a more realistic version of noise to use in simulating realistic magnetic clouds. We asked, what better source of "noise" than to use actually observed fluctuating fields associated with actual magnetic cloud's analyzed in the past? Our principle assumption was then that realistic noise fields will depend, in some way, on difference fields $\mathbf{\Delta B}$, defined as

$$\mathbf{B} = \mathbf{B_{OBS}} - \mathbf{B_M}, \tag{4}$$

based on 1-hour averages, where $\mathbf{B_M}$ is an estimated field from the force-free model of *Lepping et al.* [1990] as applied to $\mathbf{B_{OBS}}$. Since the $\mathbf{\Delta B}$s sometimes show trends of several hours duration, we refer to the noise fields developed directly from them as "trend noise" in contrast to the random noise. Figure 4 gives an example of a difference field ($\mathbf{\Delta B} = \mathbf{B_{OBS}} - \mathbf{B_M}$) for the 9 June 1997 magnetic cloud (of Figure 2) rendered in a cloud coordinate system, where $\mathbf{X_C}$ is along the cloud's axis. Various "trends" are obvious in these difference fields, especially for $\Delta B_Y'/B_O$ from 25 to 60% the way through the cloud, through about 8 points, and the first 7 points of $\Delta B_Z'/B_O$. We think of a trend as a monotonically changing field of several or more points. This kind of noise field is much more realistic for use in cloud noise simulations than the random noise. It usually suggests a profile that looks like a cloud. Figure 5 shows histograms of $\Delta B_{X,Y,Z}/B_O$ (in cloud coordinates, defined below) based on 1-hour averages from magnetic clouds from the early WIND era (1995 through most of 1998). The magnetic field data was from WIND/MFI [*Lepping et al.*, 1995] and the associated plasma data, used in the identification of these clouds and for obtaining their speed, were from WIND/SWE [*Ogilvie et al.*, 1995].

[12] The trends in the $\mathbf{\Delta B}$s may have a variety of sources, such as cloud expansion (not removed by the model), results of interaction of the clouds' boundaries with the external solar wind, occasional penetration of relatively weak interplanetary shocks, etc. As long as the amplitude of the fluctuating trend field is markedly lower than that of the variation across the cloud of the field representing the underlying ideal flux rope we assume it is reasonable to consider $\mathbf{\Delta B}$ to be "noise." We assume this, because the $\mathbf{\Delta B}$s were not accounted for by the *Lepping et al.* [1990] model, and therefore with respect to that model they are noise, even if eventually these trends are shown to have some interesting physical basis.

[13] The net simulated (S) fields ($\mathbf{B_S}$) to be tested by the model are developed by adding the exact simulated field ($\mathbf{B_{ES}}$) (as was done for the random noise study above) to the noise field:

$$\mathbf{B_S} = \mathbf{B_{ES}} + \mathbf{B_N}, \tag{5}$$

done on a 1-hour/point (average) basis. All simulated clouds will have 25 points across, which represent the average duration of 24 hours [*Lepping and Berdichevsky*, 2000]. Both $\mathbf{B_{ES}}$ and $\mathbf{B_N}$, and therefore $\mathbf{B_S}$, at this stage, are rendered in so-called magnetic cloud coordinates (X_C, Y_C, Z_C), where $\mathbf{X_C}$ (a unit vector) is aligned with the cloud's axis and positive along the direction of the axial field, $\mathbf{Z_C}$ is along the projection of the spacecraft's path on the cross-sectional plane of the cloud, and $\mathbf{Y_C} \times \mathbf{Z_C} = \mathbf{X_C}$. We point out that regardless of the actual number of hours in each real WIND cloud used to provide the $\mathbf{B_N}$ noise fields, linear interpolation of the points of the cloud's $\mathbf{\Delta B}$s provided the needed 25 noise points across the cloud, in order to be consistent with the 25 $\mathbf{B_{ES}}$ points of the exactly simulated cloud to which they are added.

[14] We will need to study as many simulated clouds as there are independent combinations of clouds formed from the $\mathbf{B_{ES}}$ and $\mathbf{B_N}$ sets. We chose 6 cases of exact clouds, $\mathbf{B_{ES}}$ sets, where the parameters to be adjusted are the longitude of the cloud axis (ϕ_{AE}, where the subscript E represents Exact) and relative closest approach distance $(Y_O/R_O)_E$. Since the local rendition of the ideal cloud is considered perfectly symmetrical about the Earth-Sun line (X_{GSE}-line), then there is no information to be gained by adjusting the latitude (θ_{AE}), i.e., all to be learned about axial direction changes are buried in ϕ_{AE}. We consider two ϕ_{AE}s, 90° and 60°, where 90° is along the Y_{GSE} axis and 60° is 30° away from that axis. We consider three $(Y_O/R_O)_E$s, 0.0, 0.3 and 0.6, where 0.0 means the spacecraft passed exactly through the cloud axis, 0.3 is 30% the way out, etc.; below we refer to $(Y_O/R_O)_E$ as CA (for exact closest approach).

[15] This initially gives us the 6 (= 2 × 3) exact clouds to which noise must be added. From the actual WIND magnetic clouds we find 19 difference field sets, where only cases of good quality fits (Q = 1 or 2) are considered (see *Lepping et al.* [2001, p. 294] concerning quality), and where a few short duration cases (durations less than 12 hours) are also discarded; one of the principal measures of quality is the χ^2 of the model's fit. These difference fields were shown to be almost bias-free, i.e., to have a small average (being 0.33 nT) when compared to typical cloud's B_O, which was found to be 16.4 nT for the WIND cloud set

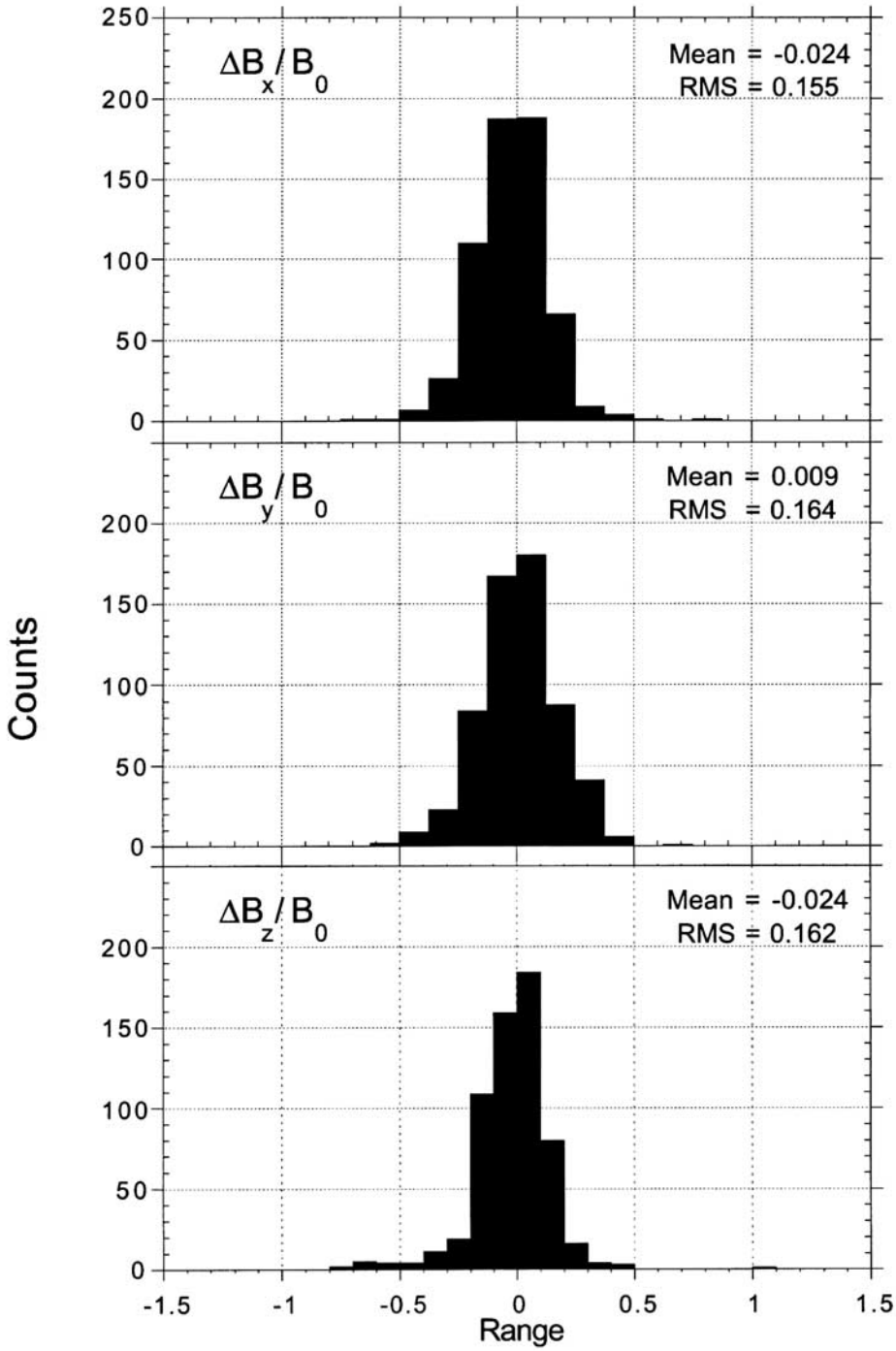

Figure 5. The $\Delta B_{X,Y,Z}$ histograms of normalized (by B_O) difference fields, defined as the difference between the field observations and the fit model's field. These represent the distribution of typical trend noise components in cloud coordinates. From these a value of $\sigma_O = 0.123$ (no units) was determined, where σ_O is the three-component average of $\Delta B/B_O$, where each cloud's individual B_Os were used in obtaining the average ratio.

[*Lepping and Berdichevsky*, 2000]. Each noise set was then made exactly bias-free in all components by subtracting its (small) average from each point. These 19 sets were then arranged to be added to the exactly simulated clouds both in a direct manner, i.e., the ''forward'' set (where point 1 of the exact cloud is to be added to point 1 of difference field, etc.) and ''backward'' (point 1 of the exact cloud is added to point 25 of difference field, point 2 to point 24, etc) giving twice as many noise sets. We then multiplied each noise set by (−1), while also retaining the original (+1) set, again doubling the number of noise sets, giving finally 76 noise sets. We note that since these sets are to be added to fixed exactly simulated magnetic clouds, we will arrive at 76 independent clouds, for a given ''noise level,'' i.e., provided that all of the

difference fields reflect the same amplitude of variation measured by their RMS deviations (sigmas). This takes us to the next step.

[16] We examined the RMS deviations of the original 19 difference fields and found that the average RMS (including all components) was close to 2.0 nT; this value was almost the same for each set to within about 3%, probably because of the manner in which the difference fields were obtained in the first place, i.e., based on cloud fitting under tight χ^2-criteria. We then forced all of the unbiased difference fields to have exactly the same RMS of 2.0 nT by choosing the needed multiplicative value for each one and by multiplying the set by it. We refer to this set as the medium noise set. To compare this to what was done in the random noise study, we notice from Table 1 and (3) that $v_{IR} = h\langle B_O\rangle\ \langle\sigma_O\rangle = 2.0\ h$ nT, where $\langle B_O\rangle = 16.4$ nT and $\langle\sigma_O\rangle = 0.123$. So for the medium noise set, h is 1.0. Note that (3) is applicable for the trend noise study as it was for that of random noise. From 76 noise sets and 6 exact clouds we obtain 456 simulated magnetic clouds at the medium noise level. We then developed three other noise sets from the medium noise set by forcing the RMS values of each noise set to be 0.5, 3, and 4 nT, which are (h =) 0.25, 1.5 and 2 times the medium noise set. We refer to these noise sets as the low, high, and very high sets, respectively. After adding these noise sets to the exact magnetic clouds, we finally arrive at 456 clouds in each of the four noise sets, giving a total of 1824 simulated magnetic clouds. Although large, this number is an acceptable burden on the cloud-fitting program. If twice as many exact clouds were generated, by examining, say, other values of ϕ_{AE} and/or $(Y_O/R_O)_E$, we would have 3648 simulated clouds to analyze in the fit program which starts to get unwieldy. It is hoped that the results from the 1824 cases can be extrapolated, at least to some extent, to account for some of the more extreme conditions of ϕ_{AE} and $(Y_O/R_O)_E$ encountered, so more simulations are probably not necessary.

[17] Since the magnetic cloud fitting program usually analyzes data in GSE coordinates, the simulated clouds must be transformed into that system from the original magnetic cloud system in which they are originally simulated. This is done by applying the following transformation matrix ($\underline{\mathbf{M}}$) to $\mathbf{B_S}$(C) to obtain $\mathbf{B_S}$(GSE) for each cloud, i.e.,

$$\mathbf{B_S}(\mathrm{GSE}) = \underline{\mathbf{M}}\mathbf{B_S}(\mathrm{C}), \tag{6}$$

where $\underline{\mathbf{M}}$ has elements m_{ij}, where i represents rows and j columns. For $\underline{\mathbf{M}}(\phi_{AE} = 90°, \theta_{AE} = 0°)$: $m_{11} = 0$, $m_{12} = 0$, $m_{13} = 1$, $m_{21} = 1$, $m_{22} = 0$, $m_{23} = 0$, $m_{31} = 0$, $m_{32} = 1$, $m_{33} = 0$, and for $\underline{\mathbf{M}}(\phi_{AE} = 60°, \theta_{AE} = 0°)$: $m_{11} = 0.500$, $m_{12} = 0$, $m_{13} = 0.866$, $m_{21} = 0.866$, $m_{22} = 0$, $m_{23} = -0.500$, $m_{31} = 0$, $m_{32} = 1$, $m_{33} = 0$. Finally, we have

$$\mathbf{B_S}(\mathrm{GSE}) = \mathbf{B_{ES}}(\mathrm{GSE}) + \mathbf{B_N}(\mathrm{GSE}). \tag{7}$$

[18] To these noised-up simulated magnetic clouds (in the form of $\mathbf{B_S}$(GSE)) we apply the *Lepping et al.* [1990] cloud model, in order to see how the 10 output parameters (listed in the Introduction, where 7 of which are actual fit parameters) are distributed about the average and about the exact input values. In particular, we are examining the RMSs (both the conventional σ_A based on the average of values and σ_E based on the known exact value, P_E) for each parameter as a function of noise level. The σs are defined as:

$$\sigma_A = (1/N)\Sigma\left(P_j - \langle P\rangle\right)^2 \quad \text{where} \langle P\rangle = (1/N)\Sigma P_j \tag{8}$$

$$\sigma_E = (1/N)\Sigma\left(P_j - P_E\right)^2 \quad \text{where j}: \ 1, .., \ N. \tag{9}$$

It can be shown that $\sigma_E{}^2 = \sigma_A{}^2 + \Delta P_{AE}{}^2$ where $\Delta P_{AE} = (P_E - \langle P\rangle)$, and where P is any one of the 10 parameters listed in the Introduction. It is expected that $\Delta P_{AE}{}^2/2\sigma_A{}^2$ will be $\ll 1.0$ for most parameters. When this is indeed the case, then

$$\sigma_E \approx \sigma_A. \tag{10}$$

Hence it usually makes little difference whether σ_E or σ_A is used for estimating the "uncertainty" on a parameter. Hence we choose to show only σ_A in any displays.

[19] Each individual parameter distribution is expected to have N = 76 individual values in it, if the program does not fail to go to completion or suffer rejected output on the basis of poor symmetry; ideal magnetic clouds should be symmetric, according to the model. On the basis of simple geometrical considerations, and since t_o is ideally supposed to be at the center of the cloud fit interval, asymmetry is measured by the asymmetry factor (ASF) defined as:

$$\mathrm{ASF} = |[1 - 2t_o/(n-1)]| \times 100\%, \tag{11}$$

(where n = 25, the actual number of points across the magnetic cloud in this case, excluding the two end points). The parameter ASF ranges from 0.0 to 100, where 0.0 is the best possible value. Hence a t_o value of 12 is the best case, where it is understood that t_o is given in terms of integral "sample times" (being 1-hour averages for most magnetic clouds), so that the ratio $2t_o/(n-1)$ is dimensionless. In practice, i.e., based on many WIND magnetic clouds, ASFs greater than about 40% are found to be unacceptable. Usually for such cases the maximum field intensity is well off center, sometimes going outside the physical range of the cloud. The ideal fit for the force-free cylindrical case demands that the maximum field be at, or reasonably close to, the center point, even if the spacecraft does not pass through the cloud's axis. Therefore for an ASF < 40%, t_o must satisfy

$$7 < t_o < 17, \tag{12}$$

(for this case of n = 25), and cases where this did not hold were not retained for further simulation analysis. Use of (11) and (12) should not significantly distort the results since in practice, as mentioned, we would not consider a magnetic cloud further if it had very poor symmetry, although cases as high as ASF = 50% have been accepted if all other aspects, such as a low $\sqrt{\chi^2}$, were acceptable.

4. Results

[20] Of the 1824 clouds simulated only 1346 were processed successfully. Eighteen simply did not converge (less than 1%); 80% of these were in the high or very high noise categories. Another 434 cases had unacceptably large

Table 2. Noise Summary: Parameter Averages and Sigmas

		Averages		Sigmas				Averages		Sigmas	
B_0, nT		PhiE = 90	PhiE = 60	PhiE = 90	PhiE = 60	R_0, 0.01 AU		PhiE = 90	PhiE = 60	PhiE = 90	PhiE = 60
Low	CA = 0	16.4	16.5	0.21	0.20	low	CA = 0	13.3	13.3	0.15	0.20
	0.3	16.5	16.5	0.35	0.46		0.3	13.3	13.3	0.20	0.22
	0.6	16.5	16.5	0.54	0.65		0.6	13.2	13.5	0.27	0.30
Medium	0.0	17.2	17.6	0.84	0.89	medium	0.0	13.4	13.4	0.67	0.81
	0.3	17.2	17.6	1.45	1.76		0.3	13.3	13.2	0.76	0.94
	0.6	17.6	17.7	2.09	2.45		0.6	13.0	13.2	1.05	1.18
High	0.0	18.3	19.3	1.30	1.56	high	0.0	13.2	13.1	0.99	1.21
	0.3	18.4	19.1	2.01	2.46		0.3	13.0	12.8	0.91	1.15
	0.6	19.1	19.6	4.09	4.26		0.6	12.4	12.4	1.84	1.88
Very high	0.0	19.7	21.4	1.78	2.28	very high	0.0	13.0	12.8	1.33	1.58
	0.3	20.0	21.2	2.81	3.19		0.3	12.7	12.3	1.25	1.39
	0.6	20.7	22.5	3.43	7.56		0.6	12.2	11.5	2.88	2.24
		Averages		Sigmas				Averages		Sigmas	
CA, R_0		PhiE = 90	PhiE = 60	PhiE = 90	PhiE = 60	t_0		PhiE = 90	PhiE = 60	PhiE = 90	PhiE = 60
Low	CA = 0	0.000	0.001	0.047	0.065	low	CA = 0	12.0	12.0	0.61	0.95
	0.3	0.316	0.317	0.044	0.060		0.3	12.0	12.0	0.65	0.97
	0.6	0.568	0.604	0.045	0.050		0.6	12.0	11.9	0.67	0.78
Medium	0.0	−0.002	−0.014	0.195	0.258	medium	0.0	12.1	11.9	1.73	2.18
	0.3	0.309	0.309	0.186	0.246		0.3	12.1	12.0	1.89	2.15
	0.6	0.572	0.605	0.180	0.201		0.6	12.0	12.0	1.93	2.18
High	0.0	−0.022	−0.035	0.286	0.389	high	0.0	12.0	11.9	1.97	2.30
	0.3	0.302	0.314	0.262	0.343		0.3	12.1	12.2	2.10	2.19
	0.6	0.620	0.676	0.446	0.471		0.6	12.0	11.9	2.12	2.13
Very High	0.0	−0.023	−0.020	0.363	0.500	very high	0.0	12.0	11.8	2.23	2.16
	0.3	0.330	0.359	0.333	0.424		0.3	12.0	11.6	2.42	2.10
	0.6	0.562	0.733	0.397	1.270		0.6	11.8	12.1	2.13	2.30
		Averages		Sigmas				Averages		Sigmas	
ϕ_A, deg		PhiE = 90	PhiE = 60	PhiE = 90	PhiE = 60	Θ_A, deg		PhiE = 90	PhiE = 60	PhiE = 90	PhiE = 60
Low	CA = 0	90.0	60.0	4.2	5.3	low	CA = 0	0.0	0.0	3.8	5.0
	0.3	88.8	59.8	4.2	5.3		0.3	0.1	−0.1	4.6	5.7
	0.6	89.2	60.0	5.0	5.7		0.6	−0.3	−0.3	4.9	5.2
Medium	0.0	89.6	58.9	16.4	21.1	medium	0.0	0.0	−0.4	10.8	12.2
	0.3	87.8	59.0	16.8	21.1		0.3	0.4	−0.1	12.6	12.4
	0.6	87.2	57.4	18.5	21.3		0.6	0.0	0.2	12.7	13.2
High	0.0	88.3	65.9	24.1	53.2	high	0.0	0.1	−1.0	13.1	14.0
	0.3	87.2	68.4	23.6	50.7		0.3	0.4	0.2	14.3	14.7
	0.6	89.8	68.2	27.5	50.5		0.6	−2.1	−0.9	19.1	18.4
Very high	0.0	88.0	69.3	30.6	59.2	very high	0.0	−0.4	−1.2	15.7	14.8
	0.3	87.8	85.7	28.2	70.2		0.3	−0.6	−3.8	18.2	17.8
	0.6	97.1	88.0	45.4	78.3		0.6	−1.9	0.2	22.0	22.9
		Averages		Sigmas				Averages		Sigmas	
E.Cone.A, deg		PhiE = 90	PhiE = 60	PhiE = 90	PhiE = 60	$\lvert\Theta_A\rvert$, deg		PhiE = 90	PhiE = 60	PhiE = 90	PhiE = 60
Low	CA = 0	5.0	6.6	2.4	3.1	low	CA = 0	2.8	3.7	2.6	3.3
	0.3	5.5	6.9	2.9	3.6		0.3	3.4	4.2	3.1	3.9
	0.6	6.3	6.9	3.1	3.5		0.6	3.8	4.0	3.1	3.3
Medium	0.0	17.9	22.4	7.8	8.9	medium	0.0	8.6	9.9	6.4	7.0
	0.3	18.9	21.9	8.9	10.3		0.3	10.0	9.8	7.6	7.5
	0.6	20.0	22.2	9.9	11.2		0.6	10.1	10.7	7.6	7.6
High	0.0	24.7	31.2	11.2	13.2	high	0.0	10.7	11.4	7.4	7.9
	0.3	24.6	29.7	12.0	14.6		0.3	11.1	11.2	8.9	9.3
	0.6	28.4	29.9	15.4	14.2		0.6	14.8	14.8	12.0	10.7
Very High	0.0	30.1	39.3	14.3	18.2	very high	0.0	12.7	11.9	9.0	8.7
	0.3	30.4	36.4	12.9	17.2		0.3	14.4	13.3	11.1	12.3
	0.6	33.9	37.0	16.4	17.8		0.6	17.1	18.5	13.8	13.2

ASFs, and finally, 26 of the remaining cases had a change of handedness which can happen when it appears (due to high noise) that the spacecraft is very far from the cloud's axis at closest approach, i.e., for Y_O/R_O of $\approx$0.95 or greater. The fit program will sometimes have difficulty determining the sign of the axial field at very large Y_O/R_Os where the axial field is very weak making the determination of handedness uncertain. So the largest cause of event dismissals was poor ASFs. It is with the remaining 1346 (successful) cases that we carry out the statistical analysis, especially to estimate averages and RMSs (σs) for various quantities. Finally since we have 6 varieties of exact magnetic clouds, 4 noise levels, and 10 parameters per cloud, we then have 240 parameter distributions, and therefore 240 resulting averages and RMSs (i.e., σ_As) of fit parameters from the cloud model program, to examine.

[21] Table 2 displays output quantities in terms of averages and σs of 6 of the fit parameters (the top six panels),

first, according to noise level, low to very high (vertically) and, second, within each noise level, according to CAs (in fractions of R_O) of 0.0, 0.30 and 0.60 (also vertically), and third, according to ϕ_{AE}s of 90° and 60° (horizontally). [Note that the Exact value of ϕ_{AE} will henceforth be called PhiE, as in Table 2, in order to differentiate it easily from the estimated (program's output) longitude angle, ϕ_A.] In the bottom two portions of the table, in the same format, we have added information on $|\theta_A|$ and the cloud axis' error cone angle, E.Cone.A, defined as the average of the angles between each estimated cloud axis of the N clouds (upon application of the fit program for some set of parameters ϕ_{AE} and $(Y_O/R_O)_E$) and the known exact cloud axis. That is,

$$\text{E.Cone.A} = (1/\text{N})\Sigma \cos^{-1}\left(\mathbf{X_{EST,j}} \cdot \mathbf{X_E}\right), (\ \text{j} = 1, ..\text{N}) \qquad (13)$$

where $\mathbf{X_{EST,j}}$ is the program-estimated cloud axis for the jth noised-up cloud, and $\mathbf{X_E}$ is the exact cloud axis; the associated sigma for the error cone angle is called σ_{ECA}. The $\mathbf{X_E}$ axis is the symmetry axis of the cone, in this usage of the term "error cone." (We point out that in some cases there were not fully 76 clouds to work with, because some were eliminated due to violation of (12). Hence in those cases N was slightly lower than 76.)

[22] We distinguish the E.Cone.A from an angle denoted by β_{ca} (which is also a cone angle), defined as the angle between the $\mathbf{X_{GSE}}$ axis and the cloud's estimated axis centered at the magnetic cloud's observing point; it is obtained by

$$\cos\beta_{ca} = \cos\theta_A \cos\phi_A. \qquad (14)$$

That is, we can think of the estimated cloud's axis as lying on the surface of a cone of angle β_{ca} whose symmetry axis is the X_{GSE} axis. Note that a similar definition could have been given for the exact cloud axis with respect to X_{GSE} axis, but it is not particularly useful here, and therefore will not be given. The β_{ca} angle is relevant for computing the effective ϕ_A, to use in estimating parameter errors in future running of the fit program when Table 2 is used. In Table 2 the averages of the fit parameters are usually close to the exact value used in the simulations, as expected, except for B_O. This is because the peak of the B_O distributions usually shifts slightly to higher values for most runs of the fit program, also as expected. From the individual subtables in Table 2 we see that for each input noise level (i.e., for v_I = 0.0, 0.5, 2.0, 3.0, and 4.0 nT) we get average (over all states) $\sqrt{\chi^2}$ fit parameters of (0.00, 0.33, 1.32, 1.95, and 2.57) $\times$ 10^{-2}, respectively. Notice that we added in the value of 0.0 for both the input noise level and for $\sqrt{\chi^2}$ representing the case of a simulated flux rope with no noise.

Table 3. Comparison of Input Trend Noise Level (v_I) Versus Output $\sqrt{\chi^2}$[a]

v_I, nT	$\sqrt{\chi^2}$	±1 σ Error	Maximum	Minimum
0.0	0.0000	0.0000	0.0000	0.0000
0.5	0.0033	0.0006	0.0039	0.0027
2.0	0.0132	0.0024	0.0156	0.0108
3.0	0.0195	0.0037	0.0232	0.0158
4.0	0.0257	0.0053	0.0310	0.0204

[a]For the average input B_O of 16.4 nT. For a given v_I, $\sqrt{\chi^2}$ was obtained from averages over the various Y_O/R_O and ϕ_A input states.

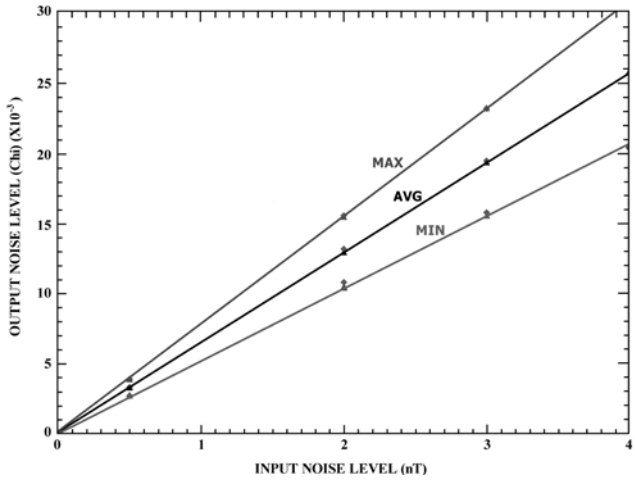

Figure 6. A comparison of output noise levels ($\sqrt{\chi^2}$) with the input random noise levels 0–4.0 nT, based on about 1800 simulated magnetic cloud $\sqrt{\chi^2}$-averages, for (top) maximum, (middle) average, and (bottom) minimum cases. A noise level of 2.0 nT yields typical $\sqrt{\chi^2}$ values (0.010 to 0.015); cloud cases of $\sqrt{\chi^2}$ greater than 0.03 are poor to very poor, and those where $\sqrt{\chi^2}$ is greater than 0.035 should be rejected. It is important to realize that these comparisons are the result of using a fixed axial B_O of 16.4 nT on the exactly simulated clouds. See color version of this figure in the HTML.

(Note that these $\sqrt{\chi^2}$ values are dimensionless, as stated above and can be related to the input noise levels only for the average input B_O of 16.4 nT.) Similarly, by examining the RMSs of each of the $\sqrt{\chi^2}$s we get (±0.0, ±0.6, ±2.4, ±3.7, ±5.3) $\times$ 10^{-3}, respectively. The average $\sqrt{\chi^2}$s combined with these RMSs give the maximums and minimums shown in Table 3, which also gives a summary of these input and output variance results. Figure 6 shows, as expected, how the $\sqrt{\chi^2}$s, and their 1 σ error limits (maximums and minimums) are also very well linearly related to the input noise levels, which we denote as v_I.

[23] Before we discuss the variations of the various fit parameters as functions of noise level, we point out a fundamental difference between estimates of the σs (uncertainties) on the quantities estimated-$_A$ and $-\phi_A$, on the one hand, and the E.Cone.A, on the other, shown in Table 2. That is, notice how the average ϕ_As are close to either 90° or 60°, but the associated sigmas grow with noise level and with PhiE, as expected. This is the same for estimated-θ_A, concerning average and sigma trends. However, the average itself for E.Cone.A grows with noise level, and similarly with respect to PhiE = 90° or 60°. Average E.Cone.A acts like a sigma itself, because of the way it was defined.

[24] Figures 7a–7c show plots of model σs, as measures of uncertainty spreads, for the various magnetic cloud fit parameters versus $\sqrt{\chi^2}$ as families of relative closest approach distances (CA of 0.0, 0.30, and 0.60) and axial directions (PhiE = 90° or 60°); the bottom two panels show averages for the cone angle and $|\theta_A|$. Figure 7a is for CA = 0.0, 7(B) for CA = 0.30, and 7(C) for CA = 0.60. (The relationship between v_I (at the top of the panels) and $\sqrt{\chi^2}$ (at the bottom) is based on the Average curve of Figure 6, where, we recall that B_O = 16.4 nT was employed in the

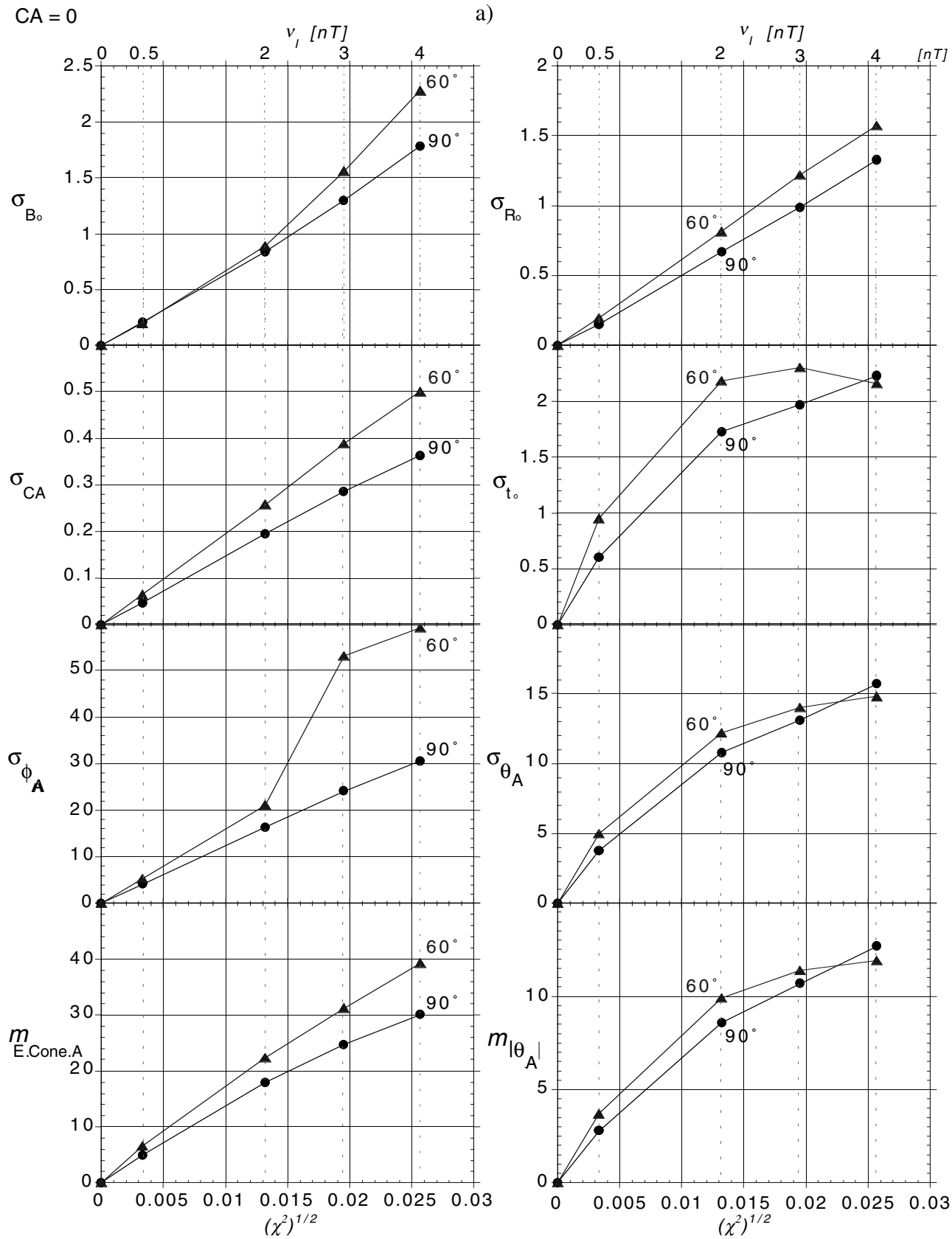

Figure 7. (a–c) Plots of model σs (i.e., measures of uncertainty spreads) for six magnetic cloud fit parameters and two related parameter averages (i.e., the cone angel and $|\theta_A|$ at the bottom) versus $\sqrt{\chi^2}$ for the fits. The input noise amplitude (v_I, in nT) is displayed as an abscissa at the top, and $\sqrt{\chi^2}$ is on the bottom abscissa. Figures 7a, 7b, and 7c refer to the CA values of 0.0, 0.30, and 0.60, respectively. See color version of this figure in the HTML.

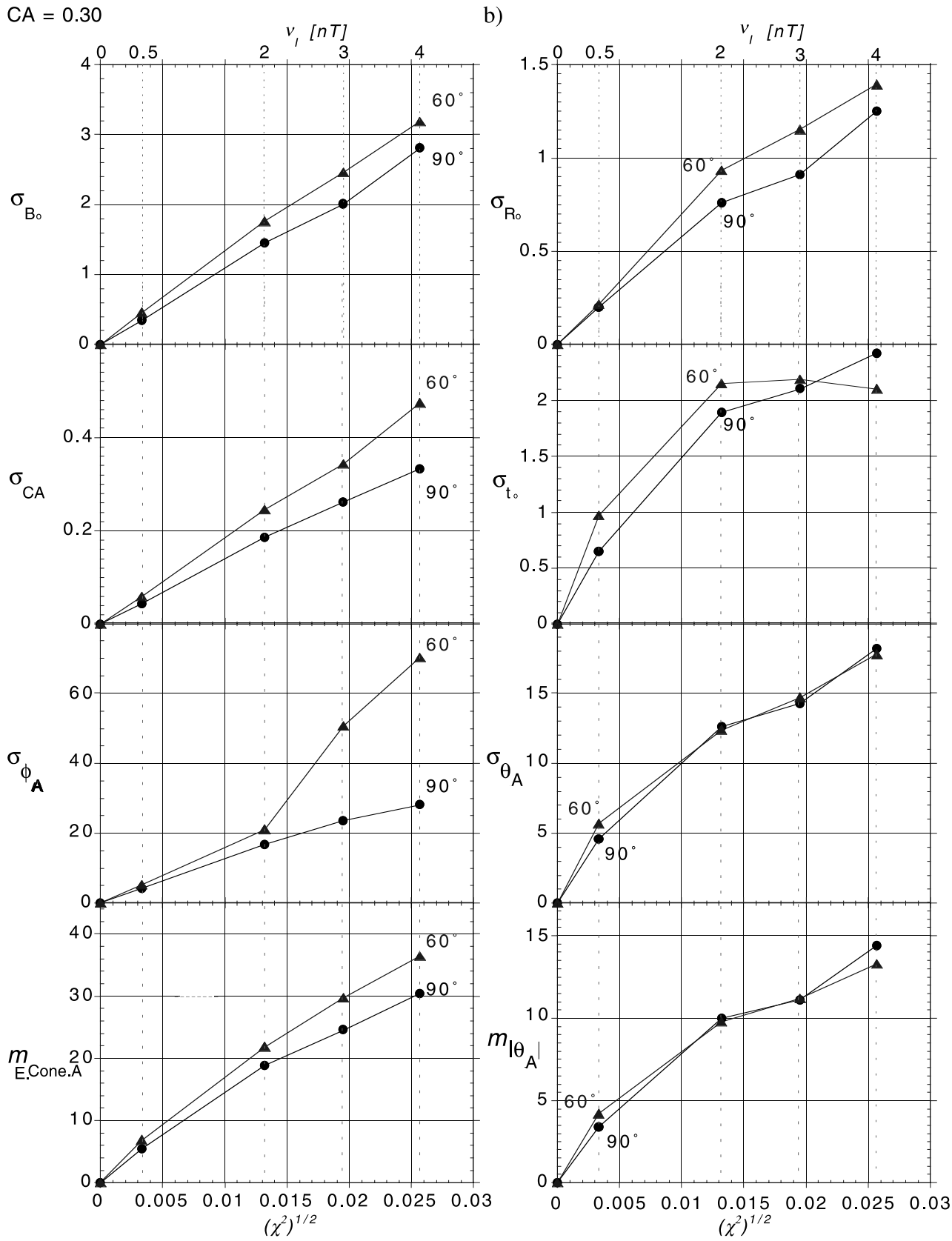

Figure 7. (continued)

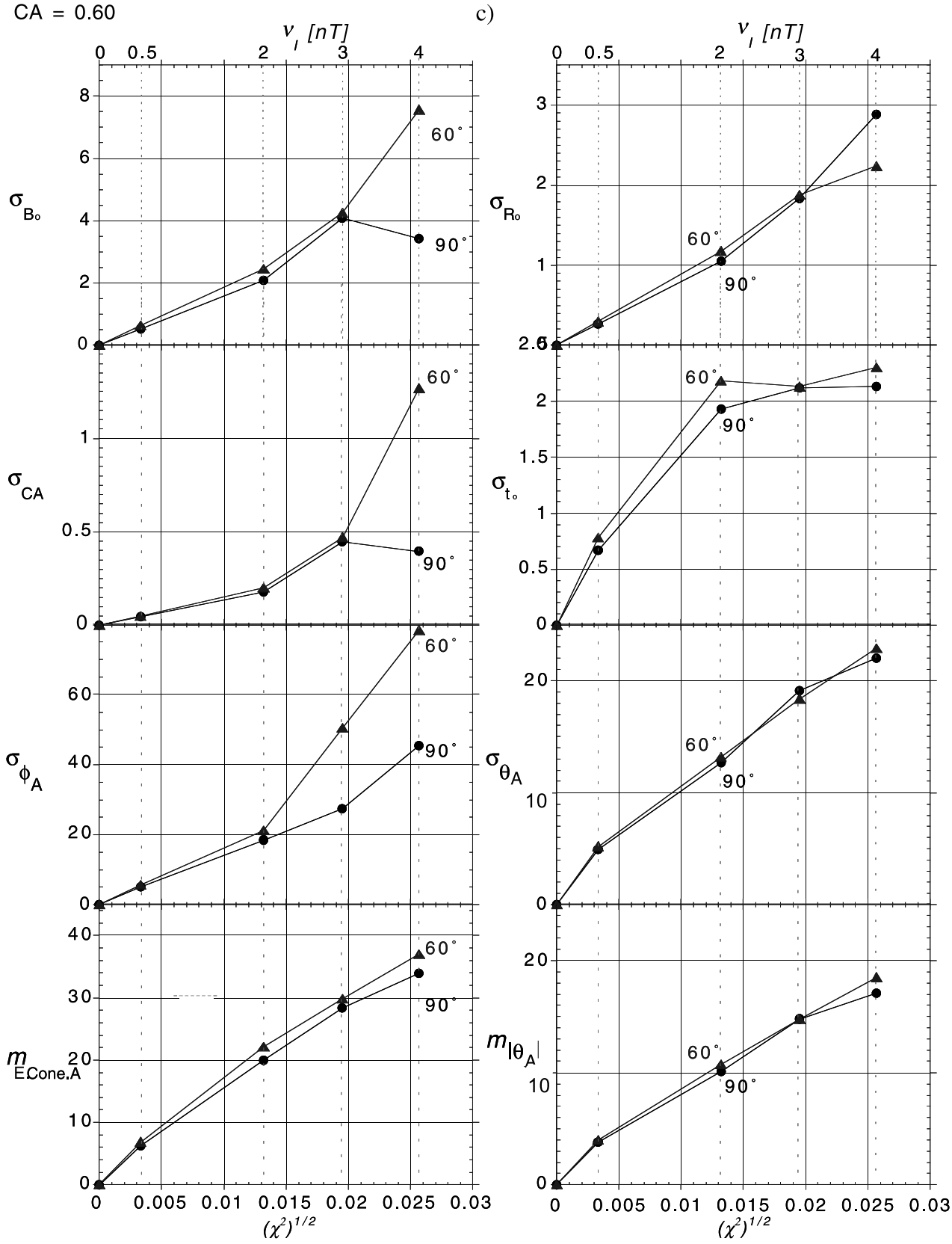

Figure 7. (continued)

simulations of the exact clouds. The units on the σs in Figure 7 are found in Table 2.) We start with Figure 7a.

[25] In all panels of Figure 7a the σs are higher for the PhiE = 60° case and deviate from each other as $\sqrt{\chi}^2$ increases. However, the $\sigma_{\phi A}$ curves deviate very markedly for v_Is of 3 and 4 nT, i.e., for high and very high noise levels. There are apparently two reasons for this: (1) we edited the simulated clouds based on the ASF which apparently has a greater effect on PhiE = 60° than for PhiE = 90°, and (2) probably of greater significance is the fact that for any significant variation of the total axial vector ϕ_A can vary greatly when θ_A gets large, and that is more likely to happen for the high and very high noise simulations. Even with all of the known merits of using a magnitude-$\theta_A - \phi_A$ coordinate display, (2) is one of its weaknesses. This is one of the reasons that we added the error cone angle (E.Cone.A) estimate of uncertainty. It is better behaved at higher noise levels and especially when θ_A is large. The other reason is that strictly it is the proper parameter to use in considering the cloud's deviation from the Y–Z(GSE) plane, not just ϕ_A. (We stress, however, that for E.Cone.A what is displayed in Figure 7 is the average (or mean = m) of the separately obtained error cone angles, all being positive. Using this mean value for measuring uncertainty in the cone angle is comparable to using the σs in θ_A and ϕ_A for measuring their uncertainties separately.) The unexpected trends in the σ_{to} curves, especially the crossover near $v_I = 4$ nT, are probably also due to the fact that we edited the simulated clouds on the basis of their values of the ASF, which depends directly on the estimated t_o, as seen in (11). The high and very high noise cases are more likely to give some poor ASFs (those outside of 40 or 50%), and since these poor cases were discarded, it is not surprising that the resulting t_o distributions, and their averages and σ_{to}s will behave irregularly. It is just another way of saying that the σ_{to}s are less trustworthy at high and very high noise levels. This is apparently also true for $\sigma_{\theta A}$ and $m_{|\theta A|}$, at least for the very high noise levels. In other words, for these high levels of cloud noise we are not able to distinguish between magnetic clouds of PhiE = 90° or 60° in estimating either $\sigma_{\theta A}$ or $m_{|\theta A|}$. It is likely that a greater number of noise sets in the simulations could have rectified this.

[26] Figure 7b for CA = 0.3 is similar to Figure 6a in most respects, but we discuss some relevant differences. An interesting difference is that the curves for PhiE = 60° and 90° for $\sigma_{\theta A}$ and $m_{|\theta A|}$ almost fall on top of each other. They essentially tell the same story. This might be expected since they measure almost the same thing, but notice that $\sigma_{\theta A}$ is always slightly greater than $m_{|\theta A|}$ for any set of conditions; this was true for the CA = 0 case in Figure 7a as well. Also at higher noise levels σ_{Bo} is more linear than it was for the CA = 0 case.

[27] Figure 7c for CA = 0.60 is also similar to 6(A) in most respects, but again we point out some relevant differences. The most striking one is that for σ_{Bo} and σ_{CA} the differences between the PhiE = 60° and 90° cases are very large, and in the case of 90°, for both parameters B_O and CA, it is probably unrealistically low for the very high noise condition. This again warns us that the usefulness of our analysis for the very high noise condition is somewhat questionable, at least for some parameters. The $\sigma_{\theta A}$ case is similar to what we obtained for the CA = 0.0 and 0.30 cases. It is interesting that, except for the σs for the three parameters B_O, CA, and ϕ_A, all σs show little difference between PhiE of 60° and 90° for the large CA of 0.60, as if asymptotic values are being reached. This may be the result of the ASF editing done earlier.

[28] Before we close discussion of the results of the trend noise study, it is instructive to compare the value of $\sqrt{\chi}^2$ (maximum = 0.0310) that is obtained for v_I of 4.0 nT with what we found for the random noise $\sqrt{\chi}^2$ (0.0185) estimation for the same v_I (then called v_{IR}), from Table 1 for a Y_O/R_O of 0%, for example. It is 1.7 times larger. Even if only the average $\sqrt{\chi}^2$ (0.0257) for the trend noise result is considered against the random noise result of 0.0185, we see a factor of 1.4 difference, and it is in the same direction. The trend noise yields more realistically appearing cloud profiles, as we have seen, and higher, more realistic $\sqrt{\chi}^2$s.

5. A Prescription for Estimating Future Model Errors

[29] This study was carried out to better understand the limitations of the *Lepping et al.* [1990] model, yielding Table 2 and Figures 7a–7c. However, it inherently provides a practical prescription for estimating the kind of errors addressed here for any magnetic cloud to be analyzed in the future, provided the model employed here is a relatively good approximation to the actual cloud's field structure. If it is not a relatively good approximation (due to cloud expansion, for example), this effect must be accommodated separately, requiring more fit parameters and presumably giving smaller errors in all parameter values. Here we describe the steps one should take to use these results for estimating 1-σ fit parameter errors upon application of the program to real magnetic clouds in the future, employing Table 2, or Figure 7 if graphical means are preferred. In either case interpolation or extrapolation may be necessary. However, if Figure 7 is used, and since it already supplies fitted curves with respect to noise for each parameter (effectively for four values of $\sqrt{\chi}^2$ in this case), interpolation is then relevant for only PhiE and Y_O (CA); then Figure 6 would not be needed in the prescription. The prescription is followed by two examples of its use. An outline of the scheme is as follows (see Appendix B for more detail on parts of the prescription):

[30] 1. Best estimates of the boundaries of the cloud are chosen and the cloud fit program is applied to the region between providing best estimated fit parameters.

[31] 2. The asymmetry factor, ASF, and $\sqrt{\chi}^2$ from the program are checked to see if they are acceptably small. Keep only the acceptable cases (see Appendix B for details on proper limits).

[32] 3. Using the estimated-θ_A and $-\phi_A$ of the cloud's axis we find a cone angle, β_{ca} (defined by (14)). β_{ca} is an effective ϕ_A. We also obtain Y_O/R_O from the fit program.

[33] 4. (If tabular values are desired.) Using the $\sqrt{\chi}^2$ value we go to Figure 6 and use it "backward" as an ordinate value to find the related abscissa value, and we quantize that to v_I = (0.0, 0.5, 2.0, 3.0, 4.0) (nT). (The AVG curve of Figure 6 is usually acceptable, or the MIN curve, to be conservative.) This provides the level of "noise" (i.e., zero, low, medium, high, or very high, respectively) to use in Table 2.

[34] 5. The proper family of parameters associated with PhiE (from estimated-β_{ca}, calculated in step 3) and Y_O/R_O are ascertained and, along with the noise level from step 4, used in Table 2/Figure 7. (See Appendix B for examples of interpolation (or extrapolation) between quantities and for a discussion of the proper care that must be taken concerning use of ϕ_A quadrants.)

[35] 6. Note that it is the σs from Table 2/Figure 7 that represent the parameter uncertainties. They represent the spreads in the model output parameters, i.e., the 1-sigma uncertainty values for most of the 7 fit parameters; handedness is not included. However, there is one exception, the E.Cone.A.; for that the average is relevant, as discussed above.

[36] 7. A special note on how to obtain the uncertainty on t_o, the estimated center time, which was derived for a case of a duration of 25 units in this study, not for actual time units. Use Table 2/Figure 7 to find t_os σ (now called σ_{to}), but a ''correction'' must be made to account for real time units which is done by using

$$\text{corrected-}\sigma_{to} = \sigma_{to} \times \text{actual duration}/24. \quad (15)$$

[37] 8. A similar adjustment must be made for B_Os sigma. That is,

$$\text{corrected-}\sigma_{Bo} = \sigma_{Bo} \times \text{actual } B_O/16.4 \text{ nT}, \quad (16)$$

where σ_{Bo} is derived from Table 2/Figure 6; note that both B_O and σ_{Bo} are in units of nT.

[38] 9. It is easy to show that the cloud's diameter, estimated in terms of the duration (ΔT) of spacecraft passage through the cloud, is given by:

$$2R_{\Delta T} = 2\sqrt{\left[Y_O{}^2 + (\sin\beta_{ca} V_C\ \Delta T/2)^2\right]}, \quad (17)$$

where the cloud is assumed to be an exact cylinder, as in the work of *Lepping et al.* [1990], and where V_C is the cloud central speed; note that this estimate takes into consideration the estimated attitude of the axis (through β_{ca} from (14)) and the estimated closest approach distance, Y_O. In judging the quality of the fit program's estimate of diameter ($2R_O$) it is useful to compare it with $2R_{\Delta T}$ from (17); note that $2R_O$ did not depend on ΔT directly.

6. Examples of Use of the Prescription

[39] We now consider two examples of magnetic clouds that we have previously studied; much interest has been given to these clouds. The first is the magnetic cloud of 18–20 October 1995 [*Larson et al.*, 1997; *Lepping et al.*, 1997; *Janoo et al.*, 1998; *Collier et al.*, 2001], based primarily on WIND data, and which in many respects is a rather typical cloud (except for its strong field). The second, because of its general importance, its very fast plasma, and topical nature, is the nontypical Bastille Day magnetic cloud of 15–16 July 2000 (date given for Earth's sighting) (*Burlaga et al.* [2001] (Voyager data); *Lepping et al.* [2001] (WIND); *Smith et al.* [2001] (ACE)]). (See *Lepping and Berdichevsky* [2000, and references therein] for typical magnetic cloud characteristics at 1 AU, for comparison.)

Table 4. October 1995 Magnetic Cloud Fit Parameters and Their Uncertainty Estimates

Parameter	Value	Uncertainty, ±1 σ	$\sigma_X/\lvert X\rvert$ (100%)[a]
Start time (year 1995)	19 Oct. (19 hours)	0.5 hour[b]	
End time	20 Oct. (00 hours)	0.5 hour[b]	
Duration, hours	30	1.0[b]	
Axial field strength (B_O)	25.6 nT	1.7 nT	6.6
Axial longitude (ϕ_A) GSE	291°	28°	15
Axial latitude (θ_A) GSE	−12°	13°	14
Cone angle	69°	24°	26
Diameter ($2R_O$, in AU)	0.263	0.020	7.4
Diameter (from duration, in AU)	0.278	0.009[b]	
Relative closest approach distance (i.e., Y_O/R_O)	0.08	0.30	30
t_o (center time, hours)	14.5	2.8	19
ASF	0.0	see uncertainty in t_o	
Handedness (for completeness)	right-handed	NA[c]	
$\sqrt{\chi^2}$	0.015	NA	

[a]All quantities are dimensionless.
[b]Estimated from sample quantization only.
[c]NA, not applicable.

[40] We start by making estimates of the uncertainties on the October 1995 magnetic cloud fit-parameters, whose values are given in the work of *Lepping et al.* [1997], based on an analysis of WIND data. The fit parameter values themselves are repeated here in the left column of Table 4. The center column shows the associated 1-σ uncertainties derived from Table 2 (or Figure 7). The ASF is excellent (0.0), and $\sqrt{\chi^2}$ (0.015) is quite good, corresponding to an AVG input v_I between 2 and 3 nT (closer to 2 nT), i.e., between medium and high noise, according to Figure 6. Since the estimated-θ_A is acceptably close to zero, we are able to use the values for estimated-ϕ_A directly from Table 2 (or Figure 7) without any need to transform the cloud's axis into the ecliptic to obtain an effective-ϕ_A (as described in Appendix B and see step 3 of the prescription), i.e., effective-ϕ_A is essentially the estimated-ϕ_A in this case. It is helpful to review how corrected σ_{to} is obtained, because it is less straightforward than the other sigmas. From Table 2 the sigma for the case of PhiE = 60°, for a 1/3 interpolation between the cases of medium and high, for CA = 0.0 (because the estimated Y_O/R_O is very small, 0.08), gives σ_{to} = 2.22. And for corrected-σ_{to} we obtain 2.22 × (30/24) hours = 2.8 hours (from (15)), where the duration was 30 hours. A PhiE = 60° is considered, because ϕ_A GSE was 291°, as Table 4 shows, and $|(291° - 360°)| = 69°$(essen-(essentially the same as β_{ca}), close enough to 60°. This is what we have referred to above as a quadrant correction: see step (5) above and Appendix B. (Actually we do an interpolation between PhiE = 60° and 90° for determining the sigma for ϕ_As uncertainty.) We now describe how the uncertainty on B_O is determined. Since the estimated B_O is 25.6 nT, but the one used to simulate the B_O table in Table 2 was 16.4 nT, we must adjust (multiply) any sigma value by 25.6/16.4, i.e., by 1.56, as dictated by (16). From the table we get an interpolated sigma of σ_{Bo} = 1.11 nT. Hence 1.11 nT × 1.56 = 1.7 nT, as Table 4 shows. Finally, we

Table 5. Bastille Day Fit Parameters and Their Uncertainty Estimates

Parameter	Value	Uncertainty, ±1 σ	$\sigma_X/\|X\|$ (100%)[a]
Start time (year 2000)	15 July (19 hours)	0.5 hour[b]	
End time	16 July (09 hours)	0.5 hour[b]	
Duration, hours	15	1.0[b]	
Axial field strength (B_O)	46.8 nT	3.3 nT	7.1
Axial longitude (ϕ_A) GSE	46°	32°	18
Axial latitude (θ_A) GSE	55°	13°	14
Cone angle	67°	25°	28
Diameter ($2R_O$, in AU)	0.348	0.020	5.7
Diameter (from duration, in AU)	0.334	0.022[b]	
Relative closest approach distance (i.e., Y_O/R_O)	0.16	0.30	30
t_o (center time, hours)	10	1.3	8.7
ASF	33%	see uncertainty in t	
Handedness (for completeness)	left-handed	NA[c]	
$\sqrt{\chi^2}$	0.0169	NA	

[a]All quantities are dimensionless.
[b]Estimated from sample quantization only.
[c]NA, not applicable.

estimate the diameter of the cloud on the basis of the duration and cloud speed, as given by (17), which is 0.278 AU; this compares well with the fit program's estimate of 0.263 AU, a 6% difference.

[41] We now order the degree of uncertainty (U) among the relative sigmas for the October 1995 case (i.e., for the ratio $U \equiv \sigma_X/|X| \times 100\%$, where X is any of the fit parameters in Table 5, and where X is replaced by 180° for the ϕ_A angle, by 90° for the θ_A and E.Cone.A, and duration is used for X for the σ of t_o. The order from best to worst is: B_O (U = 6.6%), $2R_O$ (7.4%), θ_A (14%), ϕ_A (15%), t_o (19%), E.Cone.A (26%), and Y_O/R_O (30%); these are given in the right column of Table 4. So for this magnetic cloud the axial magnetic field strength and its diameter are the most accurately estimated, and the relative closest approach distance the poorest, with the various angles and center time t_o of intermediate uncertainty. Since the values of the quantities $\sqrt{\chi^2}$, ϕ_A, θ_A, Y_O/R_O, $2R_O$, duration, and ASF were all fairly typical of magnetic clouds at 1 AU (although not quite so for B_O), this order of relative accuracy for the fit parameters will be common. It is interesting that, even though the ASF was an excellent 0.0, the error on t_o was 2.8 hours out of 30 hours duration.

[42] We now estimate the uncertainties on the fit parameters for the second Bastille Day magnetic cloud, which is referred to as MC2 in the work of *Lepping et al.* [2001], based an analysis of WIND data. The fit parameter values are given in the far right column of Table II of that paper, and a graphical representation of the fit is shown in that paper's Figure 2. We repeat a listing of most of MC2s parameter values in Table 5 here and add estimates of the uncertainties in the center column, where start and end times, duration, and handedness are also given for completeness. Again, the associated uncertainties are derived from Table 2 (or Figure 7). First, we notice that the ASF (33%) is marginally acceptable. Although the ASF is moderately large, the fit's $\sqrt{\chi^2}$ (0.0169) is very close to representing an average value corresponding to an AVG input v_I midway between 2 and 3 nT, i.e., between medium and high, according to Figure 6. Our first consideration now is what is the effective-ϕ_A (i.e., β_{ca}). Using (14) we find that $\beta_{ca} = 67°$, from $\phi_A = 46°$ and $\theta_A = 55°$ (Table 5), so values for all sigmas are again obtained by an approximate 1/3 interpolation between PhiE = 60° and 90°. (We stress that the real ϕ_A of 46° is not relevant for error estimation for nonzero θ_As; β_{ca} must be calculated and used instead.) Again we estimate the diameter of the cloud on the basis of the duration and cloud speed, as given by (17), which gives 0.334 AU; this compares well with the fit program's estimate of $2R_O = 0.348$ AU, a 4% difference. (Note that the value of 0.348 AU for the program's estimated $2R_O$ is a re-evaluation of the value of 0.378 AU given by *Lepping et al.* [2001]; it represents an ≈8% correction.) The last column of Table 5 shows the degree of uncertainty among the relative sigmas in the table by again using ratio $U \equiv \sigma_X/|X| \times 100\%$, as described above. The order from best to worst is: $2R_O$ (U = 5.7%), B_O (7.1%), t_o, (8.7%), θ_A (14%), ϕ_A (18%), E.Cone.A (28%), and Y_O/R_O (30%). These are given in the right column of Table 5; the order is similar but slightly different from that of the October 1995 case. We expect that Y_O/R_O will usually be the most poorly estimated quantity, as it was in both cases here.

7. Summary and Comments

[43] Through magnetic cloud simulations and the employment of the Monte Carlo technique, we study the degree of spread (σs) on the most probable estimations of cloud fit parameters [*Lepping et al.*, 1990], due to fluctuation/trend noise magnetic fields within actual magnetic clouds, e.g., as observed by the WIND spacecraft. For our purposes such fluctuating fields are considered to be usually the most important source of fit parameter error that can be reliably analyzed, and probably so for any specific cloud model. (Another possibly significant source of "noise" is the incorrect choice of cloud boundaries, including misidentification of a cloud. This source was only briefly discussed here.) The cloud fit model used here [*Lepping et al.*, 1990] is based on a force-free cylindrically symmetric, static (essentially meaning nonexpanding and noninteracting) magnetic cloud. The simulated clouds used in the study consist of an exact field and a noise field. We parameterize the exact part according to the direction of the cloud axis (longitudes, PhiEs of 60° and 90°) and relative closest approach distance of the observing spacecraft (three CAs ≡ Y_O/R_Os of 0.0, 0.3 and 0.6), as being likely physical quantities according to which the spreads in output quantities should depend, and the results confirmed this assumption. Four input noise levels were used representing the average level (medium) and levels 0.25, 1.5 and 2 times the medium noise set, representing low, high and very high levels. The medium characteristics of the noise were derived from actual magnetic clouds observed in the early WIND era, and because of the obvious trends seen in the noise fields they are referred to as "trend noise." (Random noise simulations were shown to be inadequate for such a study requiring unreasonably high noise amplitudes and yielding unrealistic appearing cloud profiles, as

Figure 3 with comparisons with results in Tables 1 and 3 shows). These levels were shown (Figure 6) to be linearly related to the estimations of average fit $\sqrt{\chi^2}$s, where χ^2 is the reduced chi-square measure of the quality of the fit of the model to the unit normalized magnetic field observations for 5 fit parameters (handedness and B_O, the axial field strength, are not included in this part of the fit, but are included later.) It appears that typical values of $\sqrt{\chi^2}$ are 0.013, and values of 0.035 or greater will give untrustworthy fit parameters. Hence as a result of this study we have dropped the upper limit on $\sqrt{\chi^2}$ from 0.04 to 0.035 for editing purposes.

[44] In all cases reasonable symmetry must be imposed, i.e., the ASF must be around 45% or smaller, which requires an estimated center time, t_o, in the range: of $7 < t_o < 17$, out of a full range of 25 units. It appears that typical magnetic clouds will give relative parameter error estimates in the order from best to worst of B_O, $2R_O$, θ_A, t_o, β_{ca}, and Y_O/R_O, when the *Lepping et al.* [1990] program is applied, when ASF (<45%) editing is carried out, and proper boundaries chosen.

[45] The Monte Carlo method used in this study for obtaining errors should be distinguished from the standard single value decomposition technique, which usually assumes for error estimates that, near the model solution (region of the absolute minimum of χ^2), the space of the fit parameters forms a quadratic multidimensional surface. One advantage of the Monte Carlo method as employed here is that there was no need to make any specific assumptions about the curvilinear properties of the region around the minimum in multidimensional parameter space. Also since the initial least squares part of the fit procedure in the *Lepping et al.* [1990] program is carried out using unit normalized magnetic fields for only five fit parameters of the seven (i.e., on all but B and H), as discussed earlier, a proper single value decomposition would be difficult to even define. The Monte Carlo technique was used here in connection with the fluctuation characteristics of magnetic fields of actual magnetic clouds encountered by observing spacecraft at 1 AU which we consider another advantage to the technique. The method is apparently general enough to be applicable to the uncertainties resulting from parameter fits with other magnetic cloud models, such as one with the ability to accommodate magnetic cloud (flux rope) expansion, but it would then be a more complicated model, requiring more fit parameters.

[46] A straightforward and specific 8-step prescription is given to the reader on how to utilize the results of this analysis (using Table 2/Figure 7) to estimate the $\pm 1\ \sigma$ errors on all fit parameters, and on a few other relevant parameters, for future magnetic cloud analyses. After some preliminary editing according to the degree of asymmetry, these parameter uncertainty estimations depend on the output values of the $\sqrt{\chi^2}$ value of the fit, on the relative closest approach distance, Y_O/R_O (given as CA), and on an effective-ϕ_A angle (i.e., β_{ca}). Two examples, including the second Bastille Day (July 2000) magnetic cloud [*Lepping et al.*, 2001], are given. Both examples indicate that the uncertainties on the fit parameters are medium to relatively high, but well within reasonable limits. In using this prescription we warn that the value of $\sigma_{\phi A}$ can vary greatly depending on the value of θ_A; for large $|\theta_A|$, ϕ_A and $\sigma_{\theta A}$ should be ignored and replaced by the more relevant quantities, the error cone angle (E.Cone.A), and its sigma, σ_{ECA}. The diameter $2R_O$ will usually be well estimated for those cases where the β_{ca}s are not too far from 90° and where the noise level is not too high. It can be useful to estimate the cloud's diameter based on duration and speed from (17), i.e., from $2R_{\Delta T}$. However since this estimate also depends on quantities from the fit program (i.e., θ_A, ϕ_A, and Y_O), it is not completely an independent estimate of the diameter. However, when it disagrees significantly with the estimate $2R_O$ (which is independent of duration), the disagreement provides an alert that an inconsistency in the parameters, or in our assumptions, may exist, and therefore the overall fit results or the duration for that event are uncertain. When $2R_{\Delta T}$ was compared to $2R_O$ for 40 WIND magnetic clouds, there was an average relative difference of only 16%, where about 15 poor fit quality clouds were ignored from a starting set of 55 cases; the poor quality cases were chosen, as described above, on the objective basis of the values of $\sqrt{\chi^2}$ and the ASF. This was considered satisfactory considering the complexity of the analyses and the large number of quantities involved.

Appendix A: Least Squares Fitting to Field Within Magnetic Cloud

[47] The *Lundquist* [1950] solution to $\nabla^2\mathbf{B} = -\alpha^2\mathbf{B}$ (appropriate for a cylindrically symmetric geometry [see *Priest*, 1990; *Goldstein*, 1983]), i.e., the Bessel function fields ($J_O(\alpha r)$, $J_1(\alpha r)$), $B_A = B_O\, J_O(\alpha r)$, $B_T = H\, B_O\, J_1(\alpha r)$, and $B_R = 0$, are used to simulate exact flux rope fields in cloud coordinates (see (2)), where the subscripts A, T, and R refer to axial, tangential and radial components, respectively. These functional forms are also used to least squares fit actual (or simulated) cloud fields, to obtain best estimates of fit parameters which is of concern to us here. Note that B_O is the field strength on the axis of the flux rope (cloud), and H is the handedness (left or right), or chirality, of the rope's helical field. The model field components are functions of only the radial distance from the rope's axis, r, for a fixed α. Cloud coordinates are defined in terms of the cloud's axis (i.e., by θ_A, ϕ_A) as presented in some useful system, GSE in our case. The fitting program must therefore find the axis, as well as field strength, and other relevant quantities (see Figure 1). The fitting is done in two parts. Experience dictated that best results were acquired if the direction of the field and its magnitude were fitted separately (initially using unit-normalized field), in order to estimate the five relevant geometrical quantities (θ_A, ϕ_A, Y_O, R_O, and center time, t_o); this is because the model was found to better fit the direction of the field than its magnitude.

[48] The observed field in GSE coordinates is (symbolically) transformed into an estimated cloud coordinates using $\Delta\theta_A$, $\Delta\phi_A$ through a series of iterations which after the final iteration provides the final set of θ_A, ϕ_A that relates the cloud coordinates and GSE; at this point $\Delta\theta_A$ and $\Delta\phi_A$ are unknowns. The starting values of θ_A, ϕ_A are estimated by variance analysis of the field where the intermediate variance axis is considered close to the cloud's axis. (This understanding was the result of a large number of simulations showing this to be true, but usually only so, if Y_O/R_O were not too large [*Lepping et al.*, 1990].) Then the

observed magnetic field in cloud coordinates, i.e., after such a transformation, is denoted as **Bobs,i** = (Bx,obs,i, By,obs,i, Bz,obs,i), and the model field as **Bmod,i** = (Bx,mod,i, By,mod,i, Bz,mod,i), also in cloud coordinates, both as discreet functions of time (i). For this part of the problem, the residuals are defined as follows:

$$\Delta Bi' = \sqrt{\left[(\Delta Bx, i')^2 + (\Delta By, i')^2 + (\Delta Bz, i')^2\right]}, i = 1..n,$$

where

$$\Delta Bx,i' = Bobs,x,i/Bobs,i - Bx,mod,i/Bmod,i$$
$$\Delta By,i' = Bobs,y,i/Bobs,i - By,mod,i/Bmod,i$$
$$\Delta Bz,i' = Bobs,z,i/Bobs,i - Bz,mod,i/Bmod,i,$$

(the primes denote dimensionless quantities) and where

$$Bobs, i = \sqrt{(Bx, obs, i^2 + By, obs, i^2 + Bz, obs, i^2)}$$

$$Bmod, i = \sqrt{(Bx, mod, i^2 + By, mod, i^2 + Bz, mod, i^2)},$$

i.e., the observed and model fields are separately unit-normalized, and B_O of the model field is set equal to zero at this stage, to be adjusted later; see the forms of B_A and B_T above. Because of the unit normalization of the observed and model field vectors in the above definitions of the ΔBs, they are therefore dimensionless quantities.

[49] Finally, a standard least squares algorithm attempts to minimize the sum of the squares (ssq) of the ΔBs, i.e., by minimizing

$$ssq = \Sigma_{(over\ i)}(\Delta Bi')^2, \qquad i = 1, ..n,$$

through proper adjustment of the values of $\Delta\theta_A$, $\Delta\phi_A$, Y_O, R_O, and t_o. (Strictly, t_o is replaced by an actual distance parameter, say d_o, which is related to t_o by assuming that the average speed of the cloud from the Sun during spacecraft passage through the cloud is a fixed 10^6 km/hour {= 277.8 km/s}. In this way the actual speed, V, is not needed in the analysis until the after the fitting is finished. The actual distance values for Y_O, R_O are then arrived at by multiplying the fitted values by V/277.8 km/s.) Also, we point out that fitting R_O is equivalent to fitting α since we assume that the boundary of the flux rope occurs at the first zero of J_O. Hence $J_O(\alpha R_O = 2.405) = 0.000$, or $R_O = 2.405/\alpha$. So the smaller is α, the larger is R_O for a force-free flux rope of constant α with a boundary so chosen.

[50] The fit employs an IMSL routine UNLSF, which uses the Levenberg-Marquardt algorithm to solve a nonlinear least squares problem. The input data are the trajectory, **Xi**, and observed field **Bobs,i** = (Bx,obs,i, By,obs,i, Bz,obs,i), both discreet functions of time, i. Since each of the (ΔBi′)s includes 3 independent observations (the 3 components of Bobs,i), for i = 1,.. n, and the fit has 5 parameters, the number of degrees of freedom is 3*n − 5. Thus when ssq is minimized, the more relevant ''reduced chi-square'' is defined by

$$\chi_R^2 = ssq/(3*n - 5).$$

Because the ΔBis are dimensionless, $\chi_R{}^2$ is also dimensionless.

[51] H is the handedness of the helical field, a sixth variable, and it is determined heuristically, i.e., essentially by testing to see which of +1 or −1 best provides the appropriate solution. When H is difficult to ascertain, as is usually the case for far encounters, a warning is given.

[52] Finally, B_O is computed using a 1-parameter least squares fit of the magnitudes of the model to the magnitudes of the observations. In this case, the problem is linear, and can be solved analytically. We minimize χ_B^2, where

$$\chi_B^2 = \Sigma_{(over\ i)}(Bobs, i - B_O \times Bmod, i)^2, \quad i = 1, ..n,$$

where B_O is now the only unknown. Solving the usual linear least squares problem for B_O, we find,

$$B_O = \left(\Sigma_{(over\ i)} Bobs, i \times Bmod, i\right) / \left(\Sigma_{(over\ i)} Bmod, i^2\right), i = 1, ..n.$$

Bobs and Bmod are the field magnitudes, computed as they were earlier for the residual functions. Recall that Bmod, in the initial stage, was computed using B_O set equal to 1, so now the value $B_O \times$ Bmod gives the magnitude of the model field. And now B_O is in nT. After the last iteration, and therefore when the best θ_A, ϕ_A are ascertained, they are used to transform the model field back into GSE coordinates, to be compared to the observed field, also in GSE.

Appendix B: Notes on Prescription for Estimating Model Errors

[53] The results of the Monte Carlo study on the level of uncertainty (errors) on output parameters from the *Lepping et al.* [1990] cloud fit program, developed here, can be used for estimating such errors in future applications. Such a prescription is given in a section in the text. This appendix supplements that section. First, best estimates of the boundaries of the cloud are chosen, based on the definition of a cloud as well as on the absolute value of the trial $\sqrt{\chi^2}$s obtained and on the asymmetry factor, ASF (defined by (11)). Cases where the $\sqrt{\chi^2}$ values are greater than 0.035 are usually not worth keeping. The ASF is checked to see if it exceeds 40%. If so, the estimate is rejected as being too asymmetric, i.e., the peak in |B| is too far off center. Using the estimated-θ_A and $-\phi_A$ from the fit program we develop the associated unit vector of the cloud axis and then transform it into the ecliptic plane forcing the new θ_A to be zero. We then calculate what the new ϕ_A is in this orientation. Here we call this angle the effective-ϕ_A. In actuality this angle is β_{ca} (defined by (14)). We now have a situation consistent with our simulation scheme. Effective-ϕ_A (β_{ca}) was obtained only for proper parameterization. Note that there will be a need to obtain the level of ''noise'' (i.e., low, medium, high, or very high), from Figure 6, associated with the input field parameters, before Table 2 can be used; note that Figures 7a–7c are given in terms of $\sqrt{\chi^2}$ directly. The level of noise is reflected in the value of $\sqrt{\chi^2}$ obtained in the model fit. Hence Figure 6 is applied ''backward'' by using $\sqrt{\chi^2}$, the ordinate value, usually for the AVG curve, to find the proper input v_I = [0.0, 0.5, 2.0, 3.0, 4.0] (nT), for use in Table 2. The proper family of parameters associated with PhiE and Y_O/R_O are ascertained; these are approximated by estimated-β_{ca} (i.e., by estimated-

ϕ_A) and $-Y_O/R_O$, respectively. However, likely it will be necessary to use interpolation or extrapolation for them, if the estimated-ϕ_A and estimated Y_O/R_O are far off those values chosen in these simulations. Note that "quadrant correction" will usually be necessary in determining which of PhiE = 60° or 90° is the proper value to use in Table 2. For example, if a ϕ_A is 270°, then $|(270° - 180°)| = 90°$ requires a PhiE of 90°. And, for example, if the actual ϕ_A is 210°, then $|(210° - 270°)| = 60°$ requires a PhiE of 60°. Also if the actual ϕ_A is 290° then $|(290° - 360°)| = 70°$, which is sufficiently close to 60° to use PhiE of 60°, especially since that gives a higher uncertainty level than PhiE of 90°, assuring a conservative estimate of uncertainty. Or interpolation between the PhiE of 90° and 60° values can be used, after quadrant correction, etc. (By this means we were able to keep Table 2 compact.) For the estimated β_{ca} and estimated Y_O/R_O, we find the output parameter's σs from Table 2 or Figure 7 versus $\sqrt{\chi}^2$s. The σs represent the spreads in the model output parameters, i.e., the 1-sigma uncertainty values for most of the 7 fit parameters.

[54] **Acknowledgments.** We thank the WIND/MFI and SWE teams, and in particular Keith Ogilvie (the SWE principal investigator) and Adam Szabo (the MFI data processing manager), for the care they employ in producing the magnetic field and plasma data used in part of this work, and Chin-Chun Wu for assisting in related administrative matters and for useful comments. We are also grateful to Franco Mariani (Rome) for assistance in calibrating the MFI data and Alan Lazarus for support in the analysis of the WIND magnetic clouds used in obtaining the noise data. Part of this work was done under a NASA Living With a Star (LWS) grant. Shadia Rifai Habbal thanks both referees for their assistance in evaluating this papers.

References

Berdichevsky, D. B., R. P. Lepping, and C. J. Farrugia, Geometric considerations of the evolution of magnetic flux ropes, *Phys. Rev. E*, *67*, 036405, 2003.

Bothmer, V., and R. H. Schwenn, Eruptive prominences as sources of magnetic clouds in the solar wind, *Space Sci. Rev.*, *70*, 215, 1994.

Burlaga, L. F., Magnetic clouds: Constant alpha force-free configurations, *J. Geophys. Res.*, *93*, 7217, 1988.

Burlaga, L. F., *Interplanetary Magnetohydrodynamics*, Oxford Univ. Press, New York, 1995.

Burlaga, L. F., R. P. Lepping, and J. A. Jones, Global configuration of a magnetic cloud, in *Physics of Magnetic Flux Ropes*, *Geophys. Monogr. Ser.*, vol. 58, edited by C. T. Russell, E. R. Priest, and L. C. Lee, p. 373, AGU, Washington, D. C., 1990.

Burlaga, L. F., N. F. Ness, J. D. Richardson, and R. P. Lepping, The Bastille Day shock and merged interaction region at 63 AU: Voyager 2 observations, *Sol. Phys.*, *204*, 399, 2001.

Collier, M. R., et al., Reconnection remnants in the magnetic cloud of October 18–19, 1995: A shock, monochromatic wave, heat flux drop out and energetic ion beam, *J. Geophys. Res.*, *106*, 15,985, 2001.

Farrugia, C. J., L. F. Burlaga, P. Freeman, R. P. Lepping, and V. Osherovich, A comparative study of expanding force-free constant alpha magnetic configurations with application to magnetic clouds, in *Solar Wind Seven*, edited by T. Schwenn, p. 61, Pergamon, New York, 1992.

Farrugia, C. J., et al., Uniform-twist magnetic flux tube in the solar wind, in *Solar WIND 9*, edited by S. Habbal et al., p. 745, Am. Inst. of Phys., College Park, Md., 1999.

Farrugia, C. J., et al., Multi-instrument study of the December 1996 magnetic cloud and associated interplanetary disturbances, in *The Solar Wind-Magnetosphere System-3*, edited by H. K. Biernart, C. J. Farrugia, and D. Vogl, p. 99, Austrian Acad. of Sci., Vienna, 2000.

Goldstein, H., On the field configuration in magnetic clouds, in *Solar Wind Five*, *NASA Conf. Publ. 2280*, edited by M. Neugebauer, p. 731, Greenbelt, Md., 1983.

Janoo, L., et al., Field and flow perturbations in the October 18–19, 1995, magnetic cloud, *J. Geophys. Res.*, *103*, 17,249, 1998.

Kamide, Y., et al., Magnetic storms: Current understanding and outstanding questions, in *Magnetic Storms*, edited by B. T. Tsurutani et al., p. 1, AGU, Washington D. C., 1997.

Larson, D. E., et al., Tracing the topology of the October 18–20, 1995, magnetic cloud with ~0. $1-10^2$ Kev electrons, *Geophys. Res. Lett.*, *24*, 1911, 1997.

Lepping, R. P., and D. Berdichevsky, Interplanetary magnetic clouds: Sources, properties, modeling, and geomagnetic relationship, *Recent Res. Devel. Geophys.*, *3*, 77, 2000.

Lepping, R. P., J. A. Jones, and L. F. Burlaga, Magnetic field structure of interplanetary magnetic clouds at 1 AU, *J. Geophys. Res.*, *95*, 11,957, 1990.

Lepping, R. P., et al., The WIND magnetic field investigation: The Global Geospace Mission, *Space Sci. Rev.*, *71*, 207, 1995.

Lepping, R. P., J. A. Slavin, M. Hesse, J. A. Jones, and A. Szabo, Analysis of magnetotail flux ropes with strong core fields: ISEE 3 observations, *J. Geomagn. Geoelectr.*, *48*, 589, 1996.

Lepping, R. P., et al., The Wind magnetic cloud and events of October 18–20, 1995: Interplanetary properties and as triggers for geomagnetic activity, *J. Geophys. Res.*, *102*, 14,049, 1997.

Lepping, R. P., D. Berdichevsky, and A. Szabo, Evaluation of a cylindrically symmetric force free magnetic cloud model: WIND events, *Eos Trans. AGU*, *79*(17), Spring Meet. Suppl., SH52C-02, 1998.

Lepping, R. P., et al., The Bastille day magnetic clouds and upstream shocks: Near-Earth interplanetary observations, *Sol. Phys.*, *204*, 287, 2001.

Lundquist, S., Magnetohydrostatic fields, *Ark. Fys.*, *2*, 361, 1950.

Marubashi, K., Structure of the interplanetary magnetic clouds and their solar origins, *Adv. Space Res.*, *6*(6), 335, 1986.

Marubashi, K., Interplanetary magnetic flux ropes and solar filaments, in *Coronal Mass Ejections*, *Geophys. Monogr. Ser.*, vol. 99, edited by N. Crooker et al., p. 147, AGU, Washington, D. C., 1997.

Metropolis, N., Monte Carlo: In the beginning and some great expectations, in *Lecture Notes in Physics (240), Monte-Carlo Methods and Applications in Neutronics, Photonics and Statistical Physics*, edited by R. Alcouffe et al., p. 62, Springer-Verlag, New York, 1985.

Moldwin, M. B., S. Ford, R. P. Lepping, J. A. Slavin, and A. Szabo, Small-scale magnetic flux ropes in the solar wind, *Geophys. Res. Lett.*, *27*, 57, 2000.

Ogilvie, K. W., et al., SWE, A comprehensive plasma instrument for the WIND spacecraft, The Global Geospace Mission, *Space Sci. Rev.*, *71*, 55, 1995.

Osherovich, V. A., C. J. Farrugia, and L. F. Burlaga, Dynamics of aging magnetic clouds, *Adv. Space Res.*, *13*(6), 57, 1993.

Osherovich, V. A., C. J. Farrugia, and L. F. Burlaga, The non-linear evolution of magnetic flux ropes, 2, Finite beta plasma, *J. Geophys. Res.*, *100*, 12,307, 1995.

Priest, E. R., The equilibrium of magnetic flux ropes (tutorial lecture), in *Physics of Magnetic Flux Ropes*, *Geophys. Monogr. Ser.*, vol. 58, edited by C. T. Russell, E. R. Priest, and L. C. Lee, p. 1, AGU, Washington, D. C., 1990.

Rubinstein, R. Y., *Simulation and the Monte Carlo Method*, *Wiley Ser. in Probab. and Math. Stat.*, John Wiley, Hoboken, N. J., 1981.

Schwenn, R., Mass ejections from the sun and their interplanetary counterparts, in *Solar Wind Eight, Conf. Proc.*, *328*, edited by D. Winterhalter et al., p. 426, AIP Press, Woodbury, N. Y., 1996.

Shimazu, H., and M. Vandas, A self-similar solution of expanding cylindrical flux ropes for any polytropic index value, *Earth Planets Space*, *54*, 783, 2002.

Smith, C. W., et al., ACE observations of the Bastille Day 2000 interplanetary disturbances, *Sol. Phys.*, *204*, 229, 2001.

Sobol', I. M., *A Primer for the Monte Carlo Method*, CRC Press, Boca Raton, Fla., 1994.

Tsurutani, B. T., and W. D. Gonzalez, The interplanetary causes of magnetic storms: A review, in *Magnetic Storms*, *Geophys. Monogr. Ser.*, vol. 98, edited by B. T. Tsurutani et al., p. 77, AGU, Washington, D.C., 1997.

D. B. Berdichevsky, L-3 Communications, EER Systems, Inc., Largo, MD 20774, USA. (xrdbb@lepvx3.gsfc.nasa.gov)

T. J. Ferguson and R. P. Lepping, Laboratory for Extraterrestrial Physics, NASA-Goddard Space Flight Center, Greenbelt, MD 20771, USA. (tim.ferguson@richmond.edu; ron.lepping@gsfc.nasa.gov)